MOLECULAR AND CELLULAR BIOLOGY
2023, VOL. 43, NO. 8, 371–400
https://doi.org/10.1080/10985549.2023.2227016

Taylor & Francis
Taylor & Francis Group

RESEARCH ARTICLE

The Sequential Recruitments of Rab-GTPase Ypt1p and the NNS Complex onto pre-*HAC1* mRNA Promote Its Nuclear Degradation in Baker's Yeast

Sunirmal Paira, Anish Chakraborty, Biswadip Das

Department of Life Science and Biotechnology, Jadavpur University, Kolkata, India

ABSTRACT Induction of unfolded protein response involves activation of transcription factor Hac1p that is encoded by *HAC1* pre-mRNA harboring an intron and a bipartite element (BE), which is subjected to nuclear mRNA decay by the nuclear exosome/Cbc1p-Tif4631p-dependent Exosome Targeting (CTEXT) complex. Using a combination of genetic and biochemical approaches, we demonstrate that a Rab-GTPase Ypt1p controls unfolded protein response signaling dynamics. This regulation relies on the nuclear localization of a small fraction of the cellular Ypt1p pool in the absence of endoplasmic reticulum (ER)-stress causing a strong association of the nuclear Ypt1p with pre-*HAC1* mRNA that eventually promotes sequential recruitments of NNS, CTEXT, and the nuclear exosome onto this pre-mRNA. Recruitment of these decay factors onto pre-*HAC1* mRNA is accompanied by its rapid nuclear decay that produces a precursor RNA pool lacking functional BE thereby causing its inefficient targeting to Ire1p foci leading to their diminished splicing and translation. ER stress triggers rapid relocalization of the nuclear pool of Ypt1p to the cytoplasm leading to its dissociation from pre-*HAC1* mRNA thereby causing decreased recruitment of these decay factors to precursor *HAC1* RNA leading to its diminished degradation. Reduced decay results in an increased abundance of pre-*HAC1* mRNA with intact functional BE leading to its enhanced recruitment to Ire1p foci.

KEYWORDS UPR, CTEXT, Ypt1p, nuclear exosome, *RRP6*, *CBC1*, *HAC1*

INTRODUCTION

In the nucleus of *Saccharomyces cerevisiae*, the nuclear RNA exosome and its two cofactors, TRAMP (TRf4/5p- Air1/2p-Mtr4p polyadenylation) and CTEXT (Cbc1p-Tif4631p-dependent exosome targeting) selectively degrade a diverse spectrum of aberrant messages and thereby safeguard the cells from their detrimental effects.[1–5] The nuclear exosome consists of a large multiprotein complex of 11 subunits and a few nuclear and cytoplasmic cofactors.[4,6–11] The exosome is assisted by three sets of nuclear cofactors to degrade these faulty RNAs.[12–14] The TRAMP complex provides the best-characterized example of such exosomal cofactor, which consists of a noncanonical poly(A) polymerase, Trf4p/Trf5p, a DExH box RNA helicase, Mtr4p, and the Zn-knuckle RNA binding proteins, Air1p/2p.[9,15,16] The CTEXT complex defines a second cofactor that consists of the nuclear mRNA-cap binding protein, Cbc1p/2p,[17,18] cytoplasmic nonsense-mediated decay factor Upf3p,[18,19] translation initiation factor gamma (eIF4G), Tif4631p[18,19] and a DEAD-box RNA helicase, Dbp2p. A third complex, NNS (Nrd1p-Nab3p-Sen1p), previously known to participate in the transcription termination of sn- and snoRNAs[20–24] plays a crucial role in the nuclear mRNA surveillance via the initial identification of these aberrant RNAs.[24] NNS undergoes selective cotranscriptional recruitment onto these aberrant messages by RNA polymerase II thereby

Address correspondence to Biswadip Das
biswadipdas22@gmail.com,
biswadip.das@jadavpuruniversity.in

The authors report no conflict of interest.

Received 22 December 2022
Revised 10 June 2023
Accepted 12 June 2023

"marking" them as the target for the nuclear exosome. Cotranscriptional recruitment of NNS complex onto specific aberrant message promotes the further recruitment of TRAMP and/or CTEXT depending on the na ture of aberrant transcripts that further facilitates the recruitment of the nuclear exosome to promote its decay.[24]

Previous microarray analysis directed to analyze the stability of the global messages in WT, *rrp6*-Δ, and *cbc1*-Δ yeast strains revealed that besides targeting the aberrant messages, the nuclear exosome along with its cofactor CTEXT preferentially targets and degrades approximately 200 normal mRNAs within the nucleus including the *HAC1* mRNA.[25] Notably, Hac1p is a b*ZIP* class of transcription factor that plays a pivotal role in the activation of unfolded protein response (UPR) in *S. cerevisiae* by *trans*activating the genes encoding ER chaperones.[26–29] The precursor *HAC1* mRNA harboring an intron undergoes a reversible noncanonical splicing and subsequent translation to encode Hac1p. In the absence of stress, the precursor *HAC1* mRNA remains translationally inactive via the formation of a secondary structural bridge between the intron and 5′-UTR.[30] ER stress removes the intron via the nonspliceosomal splicing that is facilitated by the ER-resident kinase-endoribonuclease Ire1p and tRNA ligase Rlg1p thereby reinstating the translation of mature *HAC1* mRNA to produce an enormous amount of Hac1p.[26–29] A crucial *cis*-acting bipartite element (BE) in the 3′-UTR of *HAC1* pre-mRNA/mRNA plays an instrumental role in recruiting/targeting this RNA to the specific intracellular foci consisting of active Ire1p, which rapidly cluster in response to stress.[29]

Apart from the nonspliceosomal splicing, the *HAC1* pre-mRNA also undergoes another layer of regulation that involves a dynamic and reversible mRNA decay by the nuclear exosome/CTEXT in the absence of ER-stress that resulted in a pool of precursor messages, most of which lack the functional BE.[31]This pre-*HAC1* transcript pool lacking BE fails to be targeted to the Ire1p foci in the absence of ER stress.[31] ER stress triggers a diminution of the 3′→5′ exosomal decay of the pre-*HAC1* transcript body thereby producing an optimum repertoire of precursor *HAC1* messages, the majority of which harbor a functional and intact BE.[31] Subsequently, this population of pre-*HAC1* mRNA with an intact/functional BE undergoes more efficient targeting and recruitment to the Ire1p clusters.[31] The nuclear exosome/CTEXT, thus, exerts a fine-tuning in the regulation of UPR signaling dynamics by facilitating the production of the functional pre-*HAC1* mRNA population with an intact BE in the absence and the presence of ER-stress.[31] However, how the precursor *HAC1* mRNA is specifically recognized and targeted for exosomal decay currently remains obscure.

A previous investigation identified a small Rab-family GTPase Ypt1p as a top interactor of *HAC1* pre-mRNA.[32] Ypt1p is an essential modulator of ER-to-Golgi transport in the secretory pathway.[33] Using an in vitro proteomic approach, these researchers demonstrated that Ypt1p binds to *HAC1* pre-mRNA in the absence of UPR activation, which facilitates its decay in the unstressed cells, and knocking down Ypt1p led to the elevated levels of *HAC1* pre-mRNA due to diminished decay.[32] However, this study did not address the mechanism of Ypt1p-dependent decay of pre-*HAC1* mRNA. While addressing the mechanism of the initial recognition and targeting of the pre-*HAC1* mRNA we explored if both the NNS complex and the Rab-GTPase Ypt1p may play any role in this process. The justification of our choice involves the established role of NNS in the initial marking of nuclear exosome target messages[24] and previously reported interaction of Ypt1p with the pre-*HAC1* mRNA in the absence of ER stress.[32] Using a combination of genetic, biochemical, and cell-biological approaches, we demonstrate that a fraction of the cellular pool of Ypt1p distributes in the nucleus in a UPR-dependent manner. This nuclear Ypt1p pool coordinates the sequential cotranscriptional recruitment of the major ESF NNS, CTEXT, and finally, the nuclear exosome onto the precursor *HAC1* mRNA in the absence of ER stress to promote its preferential degradation and thereby limits its transport and recruitment to Ire1p. ER stress promotes nucleus-to-cytoplasmic relocalization of nuclear Ypt1p pool resulting in its reduced association with pre-*HAC1* mRNA leading to diminished exosomal decay, increased targeting, and delivery of this precursor RNA to Ire1p clusters followed by

enhanced splicing and translation. This augmented translation finally results in a huge burst of Hac1p abundance, which rapidly trans activates genes encoding the ER chaperone.

RESULTS

Nrd1p promotes the recruitment of the nuclear exosome and CTEXT onto the pre-*HAC1* mRNA leading to its selective nuclear degradation. The involvement of the NNS complex in the initial identification of the exosomal RNA targets[24] let us hypothesize that this complex plays a role in the UPR signaling via initial recognition of the precursor *HAC1* message in the absence of ER stress. Recognition of pre-*HAC1* by the NNS complex would lead to subsequent recruitment of the exosome/CTEXT onto this RNA to promote its nuclear decay. To validate this postulate, we first determined the steady-state levels of pre-*HAC1* mRNA in WT and *nrd1-1* yeast strains using the RT-qPCR assay with the primer sets specific to *HAC1* intron (primer information presented in Table 1). Notably, the *nrd1-1* mutant strain harbors a premature nonsense mutation in the *NRD1* gene that leads to the formation of a truncated nonfunctional version of Nrd1p.[34,35] The data from this experiment revealed that the level of pre-*HAC1* mRNA was significantly increased in the *nrd1-1* mutant yeast strain relative to the WT strain (Fig. 1A). This finding suggests that perhaps pre-*HAC1* mRNA undergoes a diminished decay in the absence of the functional NNS complex resulting in an increased abundance of this precursor message in an *nrd1-1* strain. This observation

TABLE 1 List of primers used in this study

Primer	Oligonucleotide sequence	Gene to be amplified
OBD321	Forward 5′-GCGGGAAACAGTCTACCCTTT-3′	Pre-*HAC1* mRNA (intron-specific primer)
OBD322	Reverse 5′-CACTGTAGTTTCCTGGTCATCGTAA-3′	
OBD325	Forward 5′-ATTGACACTGCTCGTTTGTGTGT-3′	*IRE1* mRNA
OBD326	Reverse 5′-CGAGACGACAATGGGATTGA-3′	
OBD323	Forward 5′-TTTCCTGAACAAATAGAGCCATTCT-3′	*HAC1* Intron-Exon 2
OBD324	Reverse 5′-TGCGCTTCGGACAGTACAAG-3′	
OBD522	Forward 5′-ACATCGTACCGAGTGATGAACG-3′	*HAC1* Promoter
OBD523	Reverse 5′-GGCGGTTGTTGTCGTAGGTG-3′	
OBD537	Forward 5′-CGCAATCGAACTTGGCTATCCCTACC-3′	Pre- and Mature *HAC1* mRNA
OBD539	Reverse 5′-CCCACCAACAGCGATAATAACGAG-3′	
OBD184	Forward 5′-AAAGGGTGGCCCACATAAGG-3′	*CYC1*
OBD185	Reverse5′-CTTCAACCCACCAAAGGCCA-3′	
OBD272	Reverse 5′-GTGTGGATTTGATGGTATGTGTGA-3′	*LYS2*
OBD273	Forward 5′-GATATGCAGGGTCGATAACTGAAA-3′	
OBD276	Forward 5′-AGCGTCCGTAATGTCCAATTCT-3′	*NCW2*
OBD277	Reverse 5′-CCCGCACCATAAGCTATGTGA-3′	
OBD607	Forward 5′-GACAAAGGGAACGTCAACCTGAAGGGACAGAGTTTAA CCAACACCGGTGGGGGCTGCTGTTCCATGGAAAAGAGAAG-3′	Tap tagging of *YPT1* gene
OBD608	Reverse 5′-GTCTTATTTACTTATTTAGTTATTATATTATATGGGTC TGCAAGGTAGAGGCGCGCTTGTTACGACTCACTATAGGG-3′	
OBD842	HAC1-3′ΔR1 Rev-5′-TTATACCCTCTTGCGATTGTCT-3′	Construction of *HAC1*-ΔR1
OBD843	HAC1-3′ΔR1 For-5′-CTTCAACCGAAGAAGAAGAGG-3′	
OBD844	HAC1-ΔBE REv-5′-GCCAAAAAAGGGTCTTGTTC-3′	Construction of *HAC1*-ΔBE
OBD845	HAC1- ΔBE Rev-5′ TGTTTGTGTCATATCTATCTGTC-3′	
OBD846	HAC1-Strepto 3-Δ1 F-5′-TAATACGACTCACT ATAAGACAATCGCAAGAGGGTATAA-3′	Streptotag affinity purification
OBD851	HAC1-Strepto 3-Δ1 R-5′-GGATCCGACCGTGGTGCCCTTGCGGG CAGAAGTCCAAATGCGATCCCCTCTTCTTCTTCGGTTGAAG-3′	Streptotag affinity purification
OBD912	Forward R1 5′-GACAATCGCAAGAGGGTATAA-3′	Amplification for R1 region
OBD913	Reverse R1 5′-CCTCTTCTTCTTCGGTTG AA-3′	
OBD914	Forward R2 5′-TAGCTCTTGAACAAGACC-3′	Amplification for R1 region
OBD915	Reverse R2 5′-GACAGATAGATATGACACAAAC-3′	

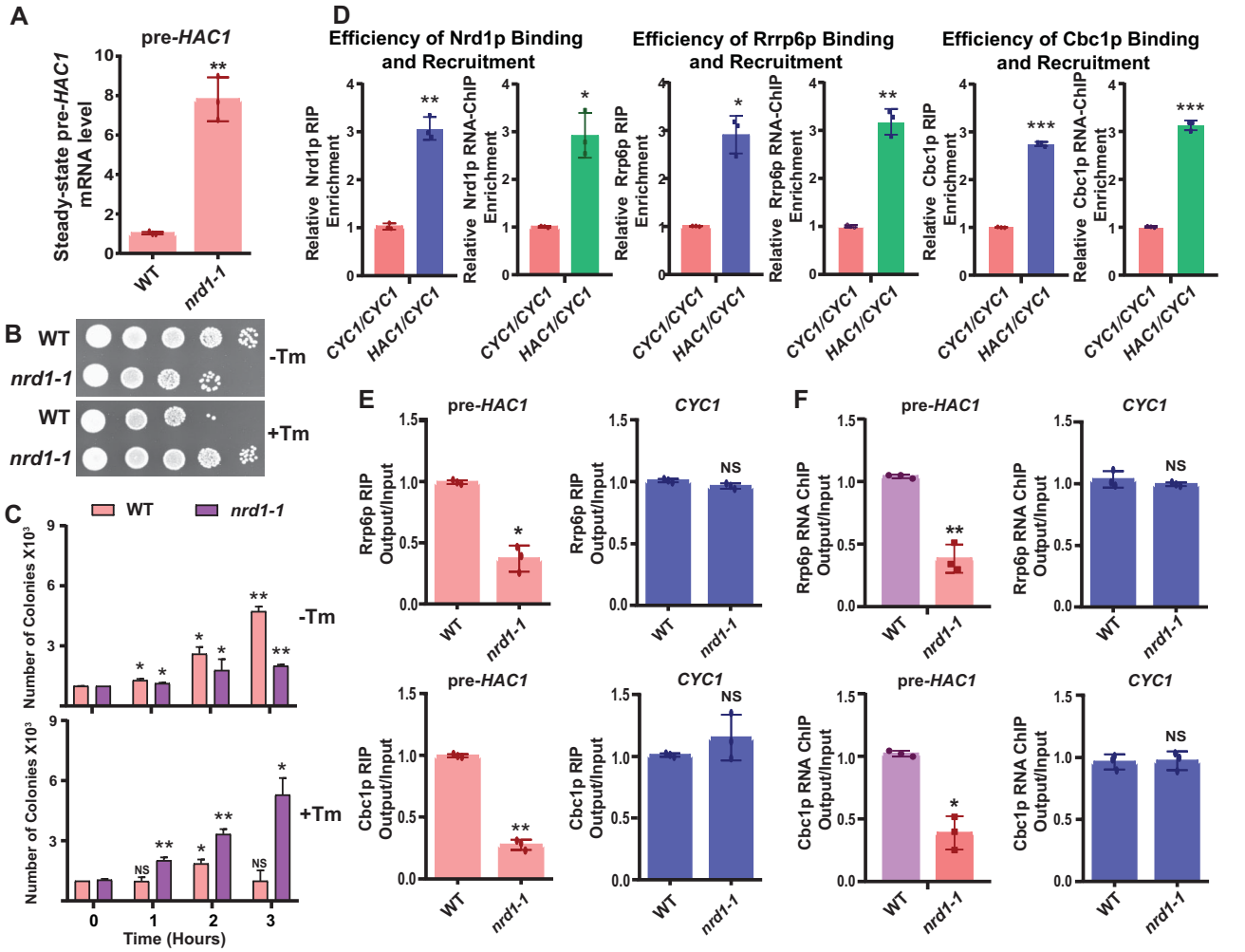

FIG 1 Nrd1p controls the UPR signaling dynamics by facilitating the cotranscriptional recruitment of exosome and CTEXT onto the precursor *HAC1* message in the absence of ER stress. (A) Histogram depicting the steady-state levels of pre-*HAC1*mRNA levels in WT (yBD-148) and *nrd1-1* (yBD-177) yeast strains using RT-qPCR analysis with a primer pair specific to *HAC1*intron. Transcript copy numbers/2 ng cDNA of each strain were normalized to *SCR1*RNA levels in respective strains and are presented as means ± SE (n = 3 for each strain). The normalized value of pre-*HAC1* mRNA from WT samples was set to one. (B) Relative growth of WT(yBD-148) and mutant *nrd1-1*(yBD-177) yeast strains in YPD solid growth media at 30 °C in the absence (-Tm) and in the presence of 1 μg/mL tunicamycin (+Tm). (C) Relative growth and survival profiles of WT (yBD-148) (orange bar) and *nrd1-1*(yBD-177) (magenta bar) strains in YPD liquid growth media either in the absence (-Tm) or in the presence of 1 μg/mL tunicamycin (+Tm) at 30 °C. (D) Relative efficiency of binding and cotranscriptional recruitment of Nrd1p, Rrp6p, and Cbc1p to the pre-*HAC1* mRNA relative to its binding and recruitment to non-UPR-specific *CYC1* mRNA in unstressed condition as determined by quantification of bound pre-*HAC1* and *CYC1* RNAs recovered from either IP following standard immunoprecipitation or RNA-chromatin-IP following RNA-ChIP assay with respective antibodies. The ratio (mean ± SE) of the abundance of pre-*HAC1* recovered from the IP relative to that of a non-ER-specific RNA is presented as relative enrichment. In each case, the abundance of a non-UPR-specific *CYC1* mRNA was set to one. (E and F) Nrd1p1p promotes the association (E), and cotranscriptional recruitment (F) of the Cbc1p and Rrp6p with/onto the pre-*HAC1* mRNA in the absence of ER-stress. For association and cotranscriptional analyses, WT (yBD-148) and *nrd1-1* (yBD-177) yeast strains, grown in the absence of tunicamycin were subjected to either RNA-IP (E) or RNA-chromatin-IP (F) respectively using anti-Rrp6p and anti-Cbc1p antibodies followed by the extraction of RNA from the IP/chromatin-IP and detection of either pre-*HAC1* or non-UPR-specific *CYC1*mRNA by RT-qPCR as described in Materials and Methods. The average of three independent experiments is shown where RIP (output) or RNA-ChIP (output) samples were normalized to input following quantification by RT-qPCR. The normalized RIP or RNA-ChIP signals obtained in the WT strain were set to one. The error bars in the graph represent standard deviations. The statistical significance of difference as reflected in the ranges of *P* values estimated from Student's two-tailed *t* tests for a given pair of test strains for each message is presented with the following symbols, *<0.05, **<0.005 and ***<0.001, NS, not significant.

further led to the speculation that the mutant *nrd1-1* strain would have a higher steady-state level of mature *HAC1* message and thus, would display a better resistance to ER stress. Subsequent examination of the relative growth profiles of WT and *nrd1-1* mutant yeast strains in the absence and in the presence of 1 μg/mL tunicamycin in both the solid (Fig. 1B) as well as the liquid (Fig. 1C) YPD medium revealed a better and more efficient growth of the *nrd1-1* strain in the presence of ER stress. This finding mimics our previous observation that yeast strains deficient in any of the nuclear decay

components, Rrp6p and Cbc1p display better growth and survival in the presence of ER stress.[31] These observations, therefore, support the idea that the NNS component Nrd1p plays a role in the UPR signaling dynamics in baker's yeast.

Next, we explored if Nrd1p indeed coordinates the recruitment of the nuclear exosome component Rrp6p and CTEXT component Cbc1p onto pre-*HAC1* mRNA. We employed RNA immunoprecipitation (RIP) and RNA chromatin-IP (RNA-ChIP) assays using specific antibodies against Rrp6p, and Cbc1p to evaluate their binding and cotranscriptional recruitment onto pre-*HAC1* RNA. To assess the specificity and authenticity of these RIP/ChIP assays, we first compared the relative efficiency of binding and recruitment of the NNS component Nrd1p onto UPR-specific pre-*HAC1* message and non-UPR-specific *CYC1* message, which showed that binding and recruitment of the NNS complex onto pre-*HAC1* are significantly higher relative to *CYC1* (Fig. 1D). Moreover, using the RIP and RNA-ChIP assays we demonstrated that binding and cotranscriptional recruitments of the exosome component Rrp6p and CTEXT component Cbc1p are also very specific to pre-*HAC1* message (Fig. 1D). Subsequently, the physical association and cotranscriptional recruitments of Rrp6p and Cbc1p with and onto pre-*HAC1* mRNA in WT and *nrd1-1* mutant strains (Fig. 1E and F, left histograms) showed that their binding and cotranscriptional recruitment was reduced by 3–4 fold in the *nrd1-1* mutant strain. These results thus demonstrated that the binding (assessed by their RIP signals) and cotranscriptional recruitment (assessed by their RNA ChIP signals) of Rrp6p and Cbc1p onto pre-*HAC1* mRNA are significantly diminished in yeast strain harboring an *nrd1-1* allele. Notably, their binding and recruitment onto non-UPR-specific *CYC1* mRNA did not alter in an *nrd1-1*strain (Fig. 1E and F, right histograms). Collectively, therefore, the above data are supportive of the view that the NNS component Nrd1p plays a crucial role in the UPR signaling by coordinating the cotranscriptional recruitment of the nuclear exosome component, Rrp6p and CTEXT component, Cbc1p onto the *HAC1* pre-mRNA in the absence of ER-stress.

Ypt1p tunes the unfolded protein response (UPR) signaling dynamics in *Saccharomyces cerevisiae*. Despite, Ypt1p regulates the steady-state level and stability of the unspliced *HAC1* mRNA in the absence of ER stress via its physical association with this RNA,[32] the mechanistic insight into the Ypt1p-dependent decay of this precursor RNA was not explored. To validate the earlier observation and to investigate the role of Ypt1p in UPR signaling systematically, we employed a temperature-sensitive mutant strain of the *YPT1* (carrying the *ypt1-3* allele) gene. We utilized this particular mutation since the same mutation was also used by[32] and this was the only mutant allele of *YPT1* gene that was available to us. Subsequently, the growth and survival profiles of the WT and *ypt1-3* mutant yeast strains were investigated in a liquid medium at various temperatures in the absence and presence of 1 μg/mL tunicamycin (Tm) (Fig. 2A). The growth profiles of the WT and *ypt1-3* strains at the permissive temperature of 25 °C in the absence of tunicamycin did not display much difference – both of them showed a similar survival profile (Fig. 2A, top left histogram). Interestingly, however, in the presence of ER stress, the *ypt1-3* strain displayed a slightly improved viability and resistance than the WT strain after a prolonged exposure to tunicamycin (Fig. 2A, top right histogram). At the non-permissive temperature of 37 °C, although the WT strain displayed a consistent growth and survival pattern in the presence and in the absence of ER stress, the survival of mutant *ypt1-3* cells was severely compromised after 2 h of temperature shift in both conditions. The number of cells that survived after 1 h following the temperature shift is significantly less (Fig. 2A, bottom histograms) thus suggesting that even a short exposure to nonpermissive temperature is fatal to these mutant cells. Importantly, their growth profiles at 30 °C in the presence of tunicamycin showed that the viability of the WT strain is significantly less after 2 and 3 h of shift relative to 1 h. The mutant *ypt1-3* strain, in contrast, displayed improved viability and resistance to ER stress relative to the WT strain even after prolonged exposure to tunicamycin (Fig. 2A, middle right histogram). Remarkably, similar survival profiles of WT and mutant *ypt1-3* strains were observed in liquid medium in the absence and presence of

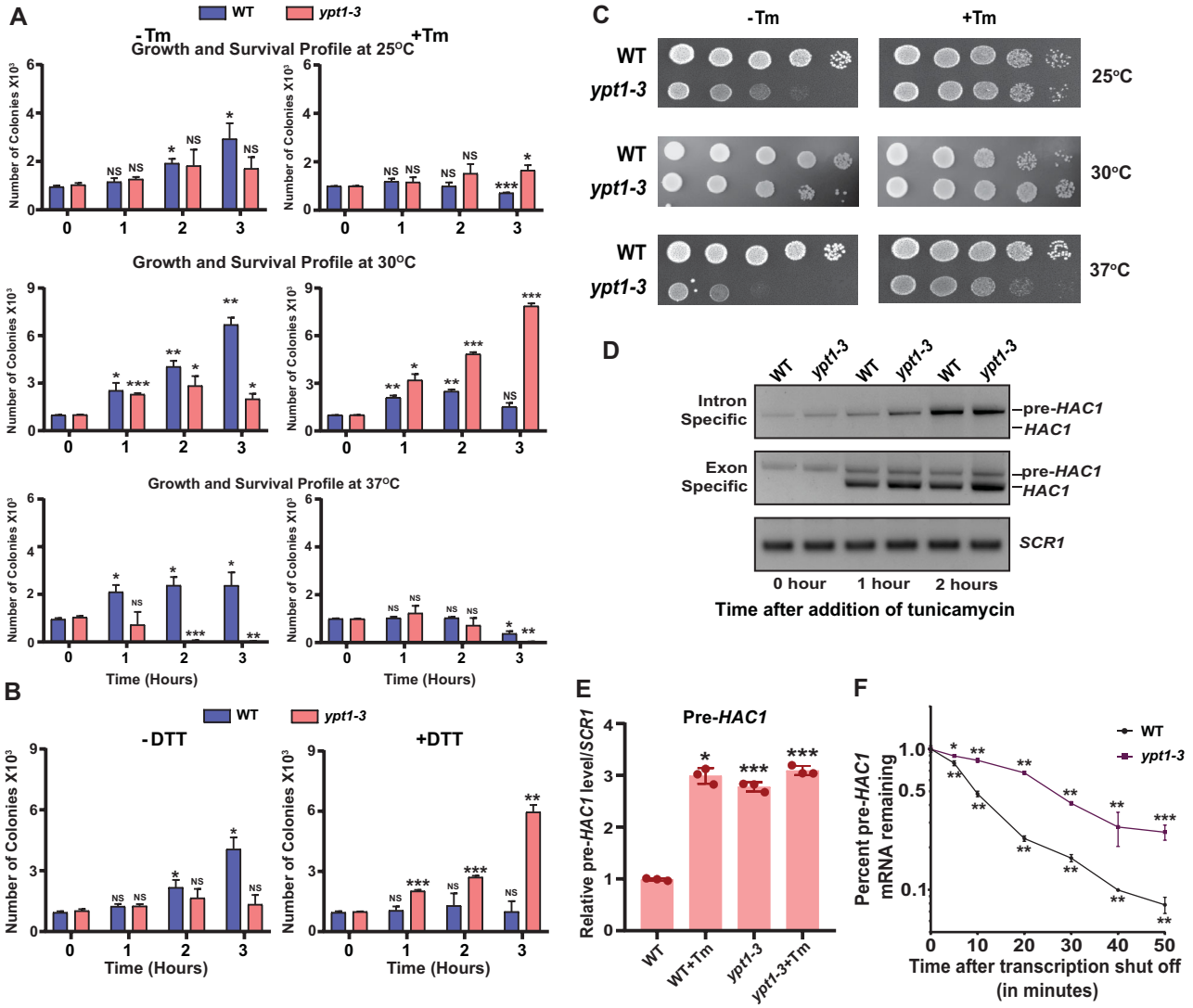

FIG 2 Ypt1p plays a vital role in the activation of UPR in baker's yeast: (A and B) Relative growth and survival profiles of WT (yBD-433) (blue bar) and *ypt1-3*(yBD-434) (orange bar) strains in YPD liquid growth media either in the absence (-Tm) or in the presence of 1 μg/mL tunicamycin (+Tm) at various temperatures (A) and in the absence (-DTT) or in the presence (+DTT) of 5 mM DTT (B).The mean of viable colonies of respective strains in each case was plotted as histograms which represent the mean of three independent experiments (n = 3) and the standard error of means (error bars). (C) Relative growth of WT (yBD-433), and *ypt1-3* (yBD-434) strains in YPD solid growth media in the absence (-Tm) and in the presence of 1 μg/mL tunicamycin (+Tm) at various temperatures. (D) Gel image depicting the relative levels of precursor and mature *HAC1* message in WT and *ypt1-3* yeast strains grown for indicated times after the addition of 1 μg/mL tunicamycin at 30 °C. The above strains were grown in the absence of tunicamycin until the OD_{600} of the culture reached 0.6 when tunicamycin was added to each culture to 1 μg/mL final concentration followed by their additional growth for indicated times. Cells were harvested from each time point and 2 ng cDNA from each cell sample was subjected to a semiquantitative PCR reaction for 32 cycles using either an intron-specific primer set (top panel, band size corresponding to pre-mRNA = 587 bp,) or an exon-specific primers-sets (bottom panel, band sizes corresponding to pre-mRNA and mature mRNA = 987 and 736 bp respectively) followed by analysis in a 1.5% agarose gel. *SCR1* (band size = 309 bp) was used as a loading control. (E) Histogram depicting the steady-state levels of precursor *HAC1* (lower panel) mRNA levels in WT (yBD-433) and *ypt1-3* (yBD-434) strains determined by RT-qPCR analysis in the absence and in the presence of 1 μg/mL tunicamycin for 2 h as described in the Materials and Methods section. Transcript copy numbers/2 ng cDNA of each strain were normalized to *SCR1* RNA levels in respective strains and are presented as means ± SE (n = 3 for each strain). The normalized value of individual mRNA from the WT strain was set to one. (F) Decay rates of pre-*HAC1* mRNA in WT (black line) and *ypt1-3* (violet line). Decay rates were determined from three independent experiments (biological replicates) by RT-qPCR analysis (using primer sets of *HAC1* intronic sequences) and the intronic signals were normalized to *SCR1* RNA signals as described in Materials and Methods. The statistical significance of difference as reflected in the ranges of *P* values estimated from Student's two-tailed *t* tests for a given pair of test strains for each message is presented with the following symbols, *<0.05, **<0.005 and ***<0.001, NS, not significant.

5 mM DTT at 30 °C (Fig. 2B) and in solid YPD medium in the absence and presence of 1 μg/mL tunicamycin at various temperatures (Fig. 2C). Data from these experiments, therefore, suggest that the mutant Ypt1-3p protein does not retain the complete function concerning its role in UPR signaling dynamics at the permissive (25 °C) and semi-restrictive/permissive (30 °C) temperatures thereby displaying mild and significant

phenotypes at 25 °C and 30 °C respectively concerning its ability to withstand ER-stress. The inability of the mutant *ypt1-3* strain to survive at the high temperature (of 37 °C) and the significant loss of function of the mutant protein at 30 °C, therefore, prompted us to select 30 °C as the appropriate temperature at which subsequent experiments involving mutant *ypt1-3* strain was carried out.

The augmented growth of the mutant *ypt1-3* strain in the presence of ER stress at 30 °C hinted at the possibility that the inactivation of the *YPT1* gene leads to the increased steady-state level of the precursor and mature *HAC1* RNA species possibly due to its diminished exosomal degradation. We validated this speculation by determining the steady-state levels of both *HAC1* precursor and mature messages at different times after the addition of tunicamycin using a semiquantitative PCR assay employing either intron-specific (detects precursor *HAC1* message) or exon-specific (detects both precursor and mature *HAC1* messages) primer sets (Fig. 2D). As shown in this figure, the levels of both the pre- and mature *HAC1* mRNA continue to increase in their steady-state levels relatively moderately in WT strain and sharply in *ypt1-3* strain at various times after the ER stress was imposed. Interestingly, the rate of increase of both of these RNA species were found to be higher in the *ypt1-3* strain relative to that in the WT strain (Fig. 2D). Higher levels of precursor and mature *HAC1* mRNAs in the *ypt1-3* strain at various times after imposition of ER stress (Fig. 2D) thus explains the ability of the mutant strain to grow and sustain better in the presence of ER stress than WT yeast strain (see Fig. 2A and B). Notably, the gradual increase in the steady-state levels of the pre-*HAC1* RNA at various times after tunicamycin addition (Fig. 2D, top panel) both in WT and *ypt1-3* strains was likely caused due to increased stability of this precursor RNA due to its diminished degradation, as observed before.[31] To establish this view, we determined the steady-state levels (Fig. 2E) and the stability (Fig. 2F) of the precursor *HAC1* message in WT and *ypt1-3* strain in the presence and absence of ER-stress using the RT-qPCR assay with the primer-sets specific to *HAC1* intron. The results of these experiments revealed that the abundance of the pre-*HAC1* mRNA population increased by about 3-fold (Fig. 2E) in the presence of ER stress in the WT strain itself. This data, thus, validates our previous finding[31] and a recent observation[36] that ER stress imposes a diminished decay of pre-*HAC1* mRNA resulting in its higher steady-state level. Notably, the steady state level of this precursor RNA was also enhanced in a *ypt1-3* mutant strain by about 3-fold in the absence and presence of tunicamycin (Fig. 2E). Consistent with this finding, a comparison of the decay rates and half-life values of pre-*HAC1* mRNA between WT and *ypt1-3* strains displayed that the decay is diminished in the *ypt1-3* strain with a concomitant enhancement of its stability by about 2.5-fold (WT half-life value = 10 min, *ypt1-3* half-life value = 27 min) (Fig. 2F). These data thus indicate that the abundance in the steady-state level of pre-*HAC1* mRNA in *ypt1-3* strain observed in Fig. 2D and E is correlative to its diminished decay rate in *ypt1-3* yeast strain. Interestingly, no significant alterations in either the steady-state levels or decay rates of three non-UPR-specific mRNAs, *CYC1*, *LYS2,* and *NCW2* in the absence and presence of ER stress were noted in the *ypt1-3* strain relative to WT (data not shown). These findings collectively suggest that Ypt1p indeed plays a vital role in modulating the UPR signaling dynamics by facilitating the decay of the pre-*HAC1* mRNA in the absence of ER-stress, which is specific and physiologically relevant thereby validating the finding from the previous report.[32]

Ypt1p promotes the nuclear decay of pre-*HAC1* mRNA by facilitating the sequential recruitment/targeting of the NNS complex, nuclear exosome, and the CTEXT complex to the premature *HAC1* mRNA in the absence of ER stress. The observation that Nrd1p coordinates the recruitment of the nuclear exosome and CTEXT onto pre-*HAC1* mRNA (Fig. 1) and Ypt1p promotes the decay of this precursor RNA (Fig. 2) let us postulate that Ypt1p facilitates the recruitment of the NNS complex, nuclear exosome/CTEXT to the pre-*HAC1* mRNA during the unstressed condition. To this end, we first query if Ypt1p interacts with the NNS complex and nuclear exosome/CTEXT by immunoprecipitation experiment using the extract prepared from the WT yeast strain

expressing N-terminally TAP tagged Ypt1p (TAP-Ypt1p) by anti-TAP antibody grown either in the absence or in the presence of tunicamycin. This was followed by the subsequent detection of the NNS components, Nrd1p/Nab3p, and exosome/CTEXT components, Rrp6p/Rrp4p and Cbc1p/Tif4631p respectively. Before carrying out the actual experiment, we first validated that the anti-TAP antibody did not yield any detectable signal when the extract from WT yeast cells expressing an untagged version of *YPT1* was used in the IP assay (data not shown). Experiments with an extract from cells expressing the TAP-tagged version of *YPT1* revealed that indeed Ypt1p displays interactions with the NNS components, Nrd1p/Nab3p, nuclear exosome components, Rrp6p/Rrp4p, and CTEXT components, Cbc1p/Tif4631p in the absence of ER-stress (Fig. 3A and C, lane 3 of each panel). Remarkably, all of these associations reduced significantly when ER stress was imposed (Fig. 3A and C, lane 2 of each panel). Importantly, mutant Ypt1-3p did not exhibit a similar interaction with any of these NNS/exosome/CTEXT components either in the absence or presence of ER stress in a similar immunoprecipitation experiment that was carried out with the extract prepared from the strain expressing the TAP-tagged version of the mutant form of Ypt1p, TAP-Ypt1-3p (Fig. 3B to D, lanes 2 and 3). Findings from these experiments thus suggest that in the absence of ER stress, Ypt1p indeed interacts with the exosome and CTEXT components, which decreased significantly, when ER stress was employed.

Next, we assessed if the physical association of Ypt1p with the nuclear exosome/CTEXT in the absence of ER-stress is physiologically meaningful, and to this end, we checked if Ypt1p (i) interacts with pre-*HAC1* mRNA in vivo in the presence and

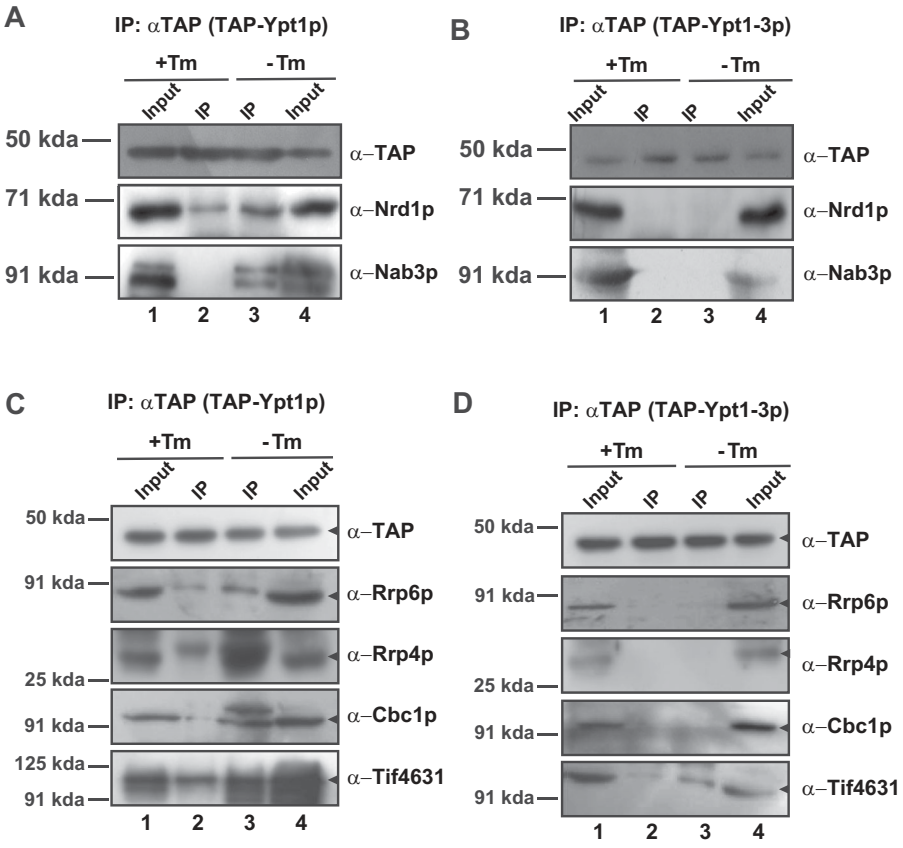

FIG 3 Ypt1p physically interacts with NNS, CTEXT, and the nuclear exosome in the absence of ER stress, which is compromised when ER stress is imposed. Immunoblots depicting the reversible physical association of either functional TAP-Ypt1p (A and B) or mutant TAP-Ypt1-3p (C and D) with NNS components Nrd1p/Nab3p (A and C), and the exosome/CTEXT components, Rrp6p/Rrp4p/Cbc1p/Tif4631p (B and D). Yeast cells expressing either WT TAP-Ypt1p (yBD-457) or mutant TAP-Ypt1-3p (yBD-565) were grown in the absence and presence of tunicamycin (1 μg/mL final concentration) followed by harvesting and preparation of cell extracts as described in Materials and Methods. TAP-Ypt1p/TAP-Ypt1-3p was precipitated by standard immunoprecipitation followed by the detection of Nrd1p, Nab3p, Rrp6p, Rrp4p, Cbc1p, and Tif4631p using their respective antibodies. The position of the nearest and relevant MW marker (in kDa) in each Western blot panel is indicated on the left.

absence of ER stress and (ii) is recruited specifically onto the pre-*HAC1* mRNA in a cotranscriptional manner. To address the first query, we carried out an RNA-immunoprecipitation (RIP) experiment from the UV-cross-linked extracts prepared from yeast strains expressing TAP-Ypt1p with an anti-TAP antibody to precipitate the TAP-Ypt1p followed by the estimation of the recovered pre-*HAC1* and three non-UPR-specific (not associated with UPR signaling) mRNAs in the immunoprecipitate (IP) using RT-qPCR (Fig. 4A). As shown in this figure, the abundance of the pre-*HAC1* mRNA recovered from the TAP-Ypt1p IP displayed a ≈ 5–6-fold enrichment relative to three non-UPR-specific mRNAs, *CYC1*, *LYS2,* and *NCW2* that could be retrieved from the same IP sample (Fig. 4A) thereby demonstrating the specificity of the Ypt1p-*HAC1* pre-mRNA interaction. Furthermore, a comparison of pre-*HAC1* mRNA bound to Ypt1p in the absence and in the presence of ER-stress showed that the abundance of the recovered pre-*HAC1* from TAP-Ypt1p IP diminished by 2-fold in the presence of ER-stress relative to unstressed WT cells (Fig. 4B, top histogram). This data suggest that the Ypt1p-pre-*HAC1* mRNA interaction becomes weakened in the presence of ER stress in a WT strain. As predicted, the levels of bound pre-*HAC1* mRNA that were recovered from the mutant TAP-Ypt1-3p IP were 2.5-fold lower in the absence and presence of ER stress than that recovered from the WT strain expressing functional Ypt1p in the absence of stress (Fig. 4B, top histogram). In addition, no significant strain-specific (WT vs *ypt1-3* mutant) or ER-stress-specific (without vs with ER-stress) differences were noted in the abundance of the non-UPR-specific *CYC1*, *LYS2,* and *NCW2* messages (Fig. 4B, three bottom histograms). These findings, together, indicate that pre-*HAC1* mRNA displays a strong and specific association with functional Ypt1p in the absence of ER stressor tunicamycin relative to other non-UPR specific messages (Fig. 4A and B) and this specific interaction was significantly diminished when tunicamycin was added. Notably, similar profiles of growth of WT and *ypt1-3* strains in the presence and in the absence of DTT (Fig. 2B), increase in the levels of pre-*HAC1* mRNA and decreased association of this RNA with Ypt1p were noted when WT strain was challenged with 5 mM DTT (data not shown). This observation led us to conclude that involvement of Ypt1p in the activation dynamics of UPR appears to be general no matter whether ER stress is generated by tunicamycin or DTT.

To further query if this binding/interaction between Ypt1p and pre-*HAC1* mRNA is forming during its nuclear transcription, we employed the RNA-chromatin-immunoprecipitation (RNA-ChIP) assay. Before carrying out the actual comparison of Ypt1p occupancy profiles onto pre-*HAC1* mRNA in various yeast strains during the ER-stress conditions by RNA-ChIP, we first determined if the ChIP signal generated from our assay procedure is highly specific. In this experiment, we used the fragmented chromatin prepared from yeast cells expressing TAP-Ypt1p that is precipitated with the anti-TAP antibody followed by quantification of the abundance of chromatin-bound pre-*HAC1* and three non-UPR specific mRNAs by qRT-PCR (Fig 4C). As shown in Fig. 4C, the abundance of the pre-*HAC1* mRNA recovered from the TAP-Ypt1p RNA-chromatin-IP samples exhibited a ≈ 3–4-fold enrichment relative to the abundance of the three other non-UPR-specific mRNAs, *CYC1*, *LYS2* and *NCW2* that could be recovered from the same chromatin-IP samples (Fig. 4C). Subsequently, the abundance of pre-*HAC1* mRNA recovered from anti-TAP RNA-chromatin-IP from the WT yeast cells in the absence of ER stress was estimated to be 2-fold higher relative to its abundance in the presence of ER stress (Fig. 4D, top histogram). Moreover, the levels of *HAC1* mRNA bound to RNA-chromatin-IP from the yeast cell expressing mutant Ypt1-3p protein with the anti-TAP antibody are ≈ 2.3-fold lower in the *ypt1-3* yeast strain relative to WT in both the absence and presence of ER-stress. As noted before, no significant strain-specific and ER-stress-specific alterations were observed in the recruitment profiles of the three non-UPR-specific, *CYC1*, *LYS2,* and *NCW2* mRNAs thereby suggesting the specificity of Ypt1p-pre-*HAC1* mRNA interaction during its Ypt1p-dependent cotranscriptional recruitment. These findings, collectively suggest that functional Ypt1p is recruited onto pre-*HAC1* mRNA in the absence of ER stress in a transcription-dependent manner, which is significantly reduced when the cells encounter ER stress.

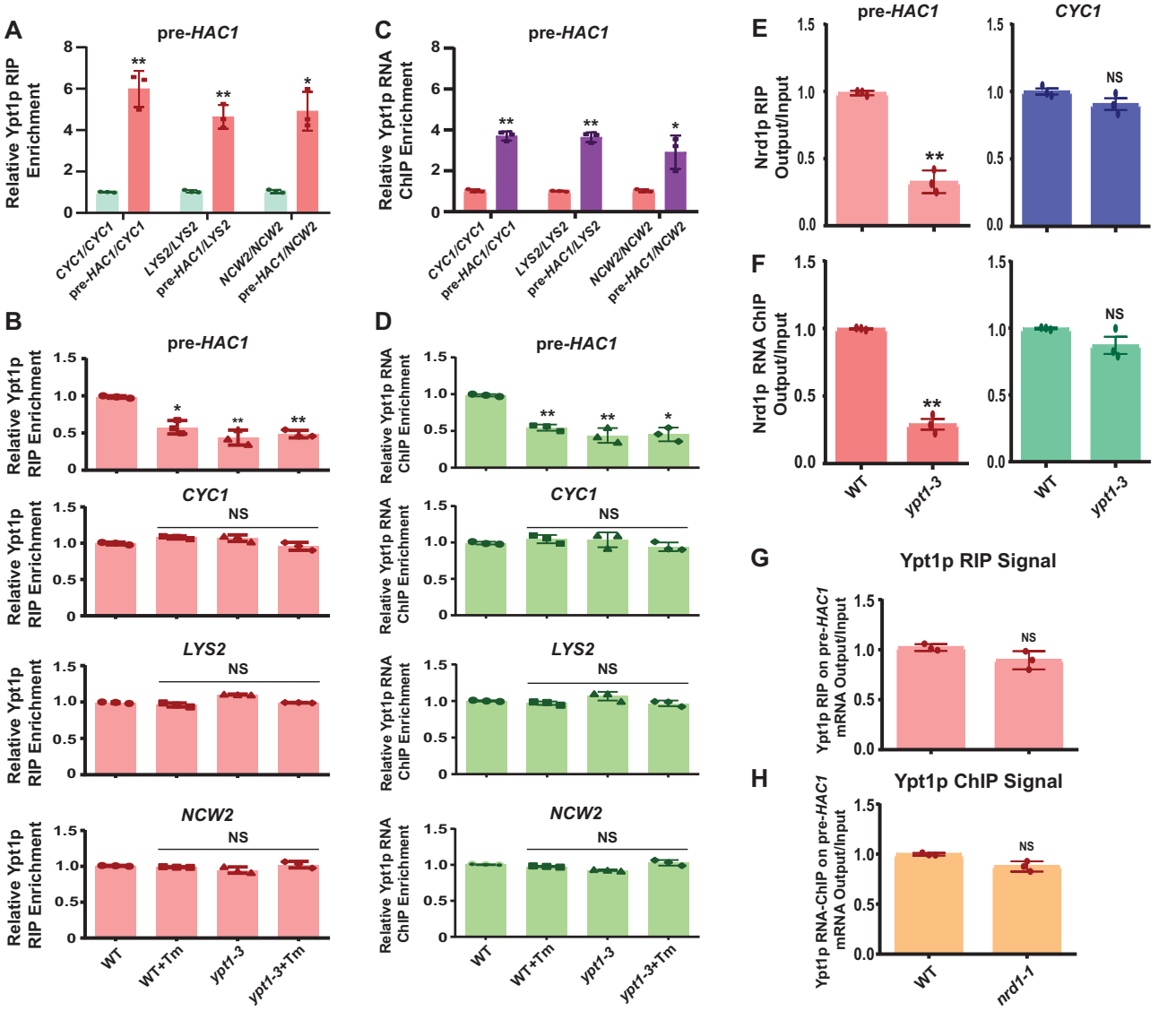

FIG 4 Ypt1p promotes the decay of precursor *HAC1* mRNA by promoting the cotranscriptional recruitment of the nuclear exosome and CTEXT onto it. (A and C) Relative efficiency of binding (A) or cotranscriptional recruitment (C) of TAP-Ypt1p to the pre-*HAC1* mRNA relative to its binding to or cotranscriptional recruitment of different non-UPR-specific mRNAs in the unstressed condition determined either by RIP (A) or RNA-ChIP (C) assay with anti-TAP antibody using an extract from yeast strain expressing TAP-Ypt1p. The ratio (mean ± SE) of the abundance of pre-*HAC1* recovered from the RIP (A) or RNA-ChIP (C) relative to that of a non-UPR-specific RNA is presented as relative Ypt1p RIP or RNA-ChIP enrichment. In each case, the abundance of a non-UPR-specific RNA was set to one. (B and D) Ypt1p selectively binds to (B) or recruited cotranscriptionally onto (D) the *HAC1* pre-mRNA in the absence of ER stress and the imposition of ER-stress weakens Ypt1p-pre-*HAC1* interaction. Extracts prepared from WT cells expressing TAP-Ypt1p (yBD-457) or mutant cells expressing TAP-Ypt1-3p (yBD-565) were grown in the absence or presence of tunicamycin (1 μg/mL) were subjected to either RIP (B) or RNA-ChIP (D) assay. Pre-*HAC1* and other non-UPR-specific messages were subsequently detected from the RNA isolated from either RIP (B) or RNA-ChIP (D) samples as described in Materials and Methods using intron-specific primer sets for *HAC1* or gene-specific primer sets. (E and F) Relative binding affinity (E) and cotranscriptional recruitment (F) of Nrd1p onto precursor *HAC1* (left histogram) and *CYC1* (right histogram) messages in WT and *ypt1-3* strains. (G and H) Relative binding affinity (G) and cotranscriptional recruitment (H) of Ypt1p on to precursor *HAC1* message in WT and *nrd1-1* yeast strains. For experiments presented in E-H, cell extracts were prepared from WT, *nrd1-1*, and *ypt1-3* yeast cells expressing TAP-Ypt1p following RNA-protein or chromatin-protein crosslinking as described before and were subjected to RIP or RNA-chromatin-IP either with anti-Nrd1p antibody (for E-F) or anti-Tap antibody (for G-H). Quantification of the bound pre-*HAC1* RNA was then estimated. The normalized value of individual pre-*HAC1* RNA recovered from the RIP/RNA-ChIP sample from the WT strain was set to one in each case. Transcript copy numbers/2 ng cDNA for each message were normalized to *SCR1* RNA levels in respective strains and are presented as means ± SE (n = 3 for each strain). Normalized values of individual mRNA from WT strain in the absence of ER stress were set to one. The statistical significance of difference as reflected in the ranges of *P* values estimated from Student's two-tailed *t* tests for a given pair of test strains for each message is presented with the following symbols, *<0.05, **<0.005, and ***<0.001, NS, not significant.

Finally, we explored whether Ypt1p functions in the upstream or downstream of the cotranscriptional recruitment event of Nrd1p onto the precursor *HAC1* message. We investigated if the selective association of Nrd1p with pre-*HAC1* mRNA and its cotranscriptional recruitment onto this precursor RNA in the absence of ER stress were affected in a strain carrying the *ypt1-3* allele. As shown in Fig. 4E and F, the binding of Nrd1p to the pre-*HAC1* message as well as its co-transcriptional recruitment were reduced by approximately 3.5–4-fold in a yeast strain harboring the *ypt1-3* allele, thus suggesting that functional Ypt1p plays a key role in the subsequent recruitment of Nrd1p onto pre-*HAC1* message (Fig. 4E and F). To further reinforce this idea, we also carried out reciprocal RIP and RNA-ChIP experiments to see if the mutation in the *NRD1* gene could impair the recruitment of Ypt1p. As shown in Fig. 4G and H, neither the binding of Ypt1p nor its recruitment onto the pre-*HAC1* message was compromised in a yeast strain carrying the *nrd1-1* allele (Fig. 4G and H). All these observations, thus, collectively suggest that in the absence of ER stress, the co-transcriptional recruitment of Ypt1p onto pre-*HAC1* message takes place upstream of the Nrd1p recruitment. Thus, Ypt1p plays a key role in the initial recognition of the pre-*HAC1* message that is characterized by its recruitment onto this precursor message. Most remarkably, this event further promotes the sequential recruitments of Nrd1p/NNS, CTEXT, and the nuclear exosome to facilitate the rapid nuclear decay of this precursor message in the absence of ER stress. ER stress leads to the diminished cotranscriptional recruitment and binding of Ypt1p onto this precursor RNA, which is followed by the compromised recruitments of all the decay factors downstream thereby leading to its diminished degradation.

Ypt1p promotes the targeting and recruitment of the pre-*HAC1* mRNA to the Ire1 foci. Involvement of the Rab-GTPase Ypt1p in the dynamic and reversible nuclear decay of *HAC1* pre-mRNA encouraged us to interrogate if Ypt1p also governs the targeting of the pre-*HAC1* mRNA from its transcription site and influences its successful recruitment to the Ire1p foci. We validated this query by determining the intracellular distribution of *HAC1* mRNA in WT and *ypt1-3* yeast strains. Both of these strains coexpress $HAC1^{NRE}$ mRNA (an engineered version of *HAC1* construct carrying an RNA aptamer with a 22 nt RNA module identical to the nucleolin recognition element, NRE), a nucleolin-GFP fusion protein, and Ire1p-RFP (Ire1p protein tagged with RFP)[37] using confocal imaging. The *in situ* distribution/localization of pre-$HAC1^{NRE}$ RNA bound nucleolin-GFP ($HAC1^{NRE}$-nucleolin-GFP) fusion protein, and Ire1p-RFP (Fig. 5A, see merge and DIC/merge panel in the top row) reveals that in *ypt1-3* cells, where Ypt1p is not functioning optimally, the abundance of green (GFP) signal representing the *HAC1* message is visibly more than the WT yeast strain (Fig. 5A, *HAC1* mRNA panel). Furthermore, in the WT strain, the most of the green ($HAC1^{NRE}$-*GFP* mRNA) spots/signals appear to be excluded from the red (Ire1p-RFP) spots representing localized Ire1p clusters. In the *ypt1-3* mutant strain, in contrast, a comparison of the distribution of pre-$HAC1^{NRE}$ bound Nucleolin-GFP and Ire1p-RFP revealed the presence of more abundant yellow spots that resulted from the overlapping $HAC1^{NRE}$-*GFP* and Ire1p-RFP signals (Fig. 5A, see merge and DIC/merge panel in bottom row). This finding thus indicates that the pre-*HAC1* message is more efficiently targeted to the Ire1p foci in the *ypt1-3* mutant yeast strain.

To bolster this finding, we estimated the extent of the colocalization of the signal intensities of $HAC1^{NRE}$-Nucleolin-GFP and the Ire1p-RFP in both WT and *ypt1-3* yeast strains. The colocalization index is very low in WT yeast strain (CI $= 0.28 \pm 07$) (Fig. 5B, colocalization data provided in Table 2), which is manifested by the presence of very few yellow spots (merged panel in the top row in Fig. 5A). A careful examination of their distribution/localization in *ypt1-3* strain (merged panel bottom row in Fig. 5A) further revealed more intense as well as frequent colocalization of $HAC1^{NRE}$-Nucleolin-GFP signal with the Ire1p-RFP (representing the cellular distribution of Ire1p foci) (CI $= 0.65 \pm 0.13$) (Fig. 5B, colocalization data provided in Table 2). This finding argues that a higher and more efficient targeting and recruitment of the precursor-*HAC1*

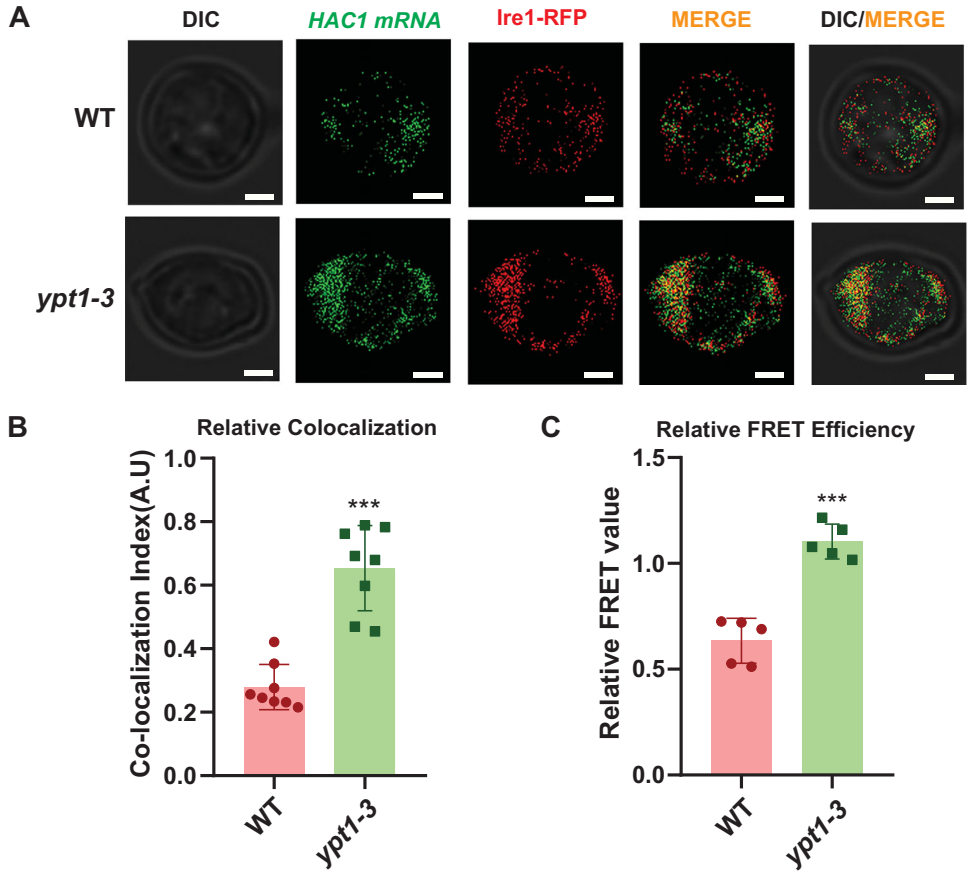

FIG 5 Ypt1p controls the targeting and recruitment of pre-*HAC1* mRNA to the Ire1p foci. (A) Localization of *HAC1*^{NRE} mRNA decorated with *NRE-GFP2* and Ire1-RFP following the induction of ER stress by 1 μg/mL tunicamycin for 30 min in WT and *ypt1-3* yeast strains. The images were captured and processed as described in Materials and Methods. The white bar in each image panel indicates two micrometers. (B) Histogram depicting the colocalization index of *HAC1*^{NRE}-GFP-nucleolin mRNA signal and Ire1p-RFP signal at 30 min after imposition of ER stress by 1 mg/mL tunicamycin in WT and *ypt1-3* yeast strains. Colocalization index for *HAC1*^{NRE}-GFP-nucleolin recruitment into Ire1 foci was expressed in arbitrary units. Colocalization data are presented in Table 2. (C) Relative fluorescence resonance energy transfer (FRET) between *HAC1*^{NRE}-GFP-nucleolin and Ire1p-RFP in WT and *ypt1-3* yeast strains. Quenching of donor *HAC1* ^{NRE}-GFP-nucleolin mRNA in the presence of Ire1p-RFP (acceptor) in WT and *ypt1-3* strains was determined as described in Materials and Methods. Histogram depicting the relative FRET value (in arbitrary units) from donor *HAC1*^{NRE}-GFP-nucleolin mRNA into Ire1p-RFP foci at 30 min after induction of ER stress by 1 μg/mL tunicamycin in a WT and *ypt1-3* strains. Donor (*HAC1*^{NRE}-GFP-nucleolin mRNA) quenching as an indicator of relative FRET value was measured for *HAC1*^{NRE}-GFP-nucleolin recruitment into Ire1p foci. The means and standard errors of the mean were determined from n = 3 (three independent biological replicates). Donor quenching estimated by flow cytometry from 10,000 cells of each strain was determined as described in the Materials and Methods section using BD FACS Verse software. FRET data are presented in Table 3. The statistical significance of difference as reflected in the ranges of *P* values estimated from Student's two-tailed *t* tests for a given pair of test strains is presented with the following symbols, *<0.05, **<0.005 and ***<0.001, NS, not significant.

TABLE 2 Colocalization index of WT and *ypt1-3* yeast strains (Data associated with Fig. 5B)

	Colocalization Index	
Sample	**WT**	***ypt1-3***
1	0.2314 (Mean value from Replicate 1)	0.7891(Mean value from Replicate 1)
2	0.2765 (Mean value from Replicate 2)	0.6792 (Mean value from Replicate 2)
3	0.3532 (Mean value from Replicate 3)	0.7623 (Mean value from Replicate 3)
4	0.4213 (Mean value from Replicate 4)	0.4543 (Mean value from Replicate 4)
5	0.2341 (Mean value from Replicate 5)	0.7832 (Mean value from Replicate 5)
6	0.2156 (Mean value from Replicate 6)	0.4698 (Mean value from Replicate 6)
7	0.2451 (Mean value from Replicate 7)	0.5981 (Mean value from Replicate 7)
8	0.2561 (Mean value from Replicate 8)	0.6923 (Mean value from Replicate 8)
The mean of all replicates	0.2791	0.6535

mRNA to the Ire1p foci takes place in a yeast strain carrying the *ypt1-3* allele as predicted by our hypothesis. It should be noted here that the allele encoding *HAC1*^{NRE} mRNA is biologically functional which was confirmed previously.[31]

To further corroborate the role of Ypt1p in controlling the targeting and recruitment of pre-*HAC1* messages, we also evaluated the relative proximity of the *HAC1*^{NRE}-nucleolin-GFP RNA and Ire1p-RFP moiety by determining the fluorescence resonance energy transfer (FRET) from *HAC1*^{NRE}-nucleolin-GFP (donor) to Ire1p-RFP fluorophore (acceptor). Fluorescence quenching of the donor *HAC1*^{NRE}-nucleolin-GFP was determined as an indicator of FRET in WT and *ypt1-3* yeast strains at 30 min after the addition of tunicamycin. As shown in Fig. 5C, a 2-fold higher donor *HAC1*^{NRE}-nucleolin-GFP quenching due to a higher FRET from *HAC1*^{NRE}-nucleolin-GFP to Ire1p-RFP was detected in the *ypt1-3* strain relative to FRET value obtained in the WT strain at 30 min after the ER stress was imposed (Fig. 5C) (FRET efficiency data of WT and *ypt1-3* strains are provided in Table 3). Notably, a similar increase in FRET signal was previously observed in the *cbc1-*Δ mutant yeast strains deficient in CTEXT component Cbc1p relative to WT yeast strains[31] under similar ER-stressed conditions. This finding, thus, argues a closer physical proximity between the *HAC1*^{NRE}-nucleolin-GFP and Ire1p-RFP in the *ypt1-3* strain, thereby implying that more *HAC1* precursor mRNA is efficiently recruited onto the active Ire1p clusters in the *ypt1-3* strain. Together, these findings support the conclusion that in the absence of ER stress, the abundance of the precursor-*HAC1* mRNA with intact BE is dictated by the Ypt1p via cotranscriptional recruitment of the NNS/CTEXT/exosome complex onto this precursor message. Recruitment of these decay factors promotes its nuclear decay, thereby resulting in a population of pre-*HAC1* transcripts most of which lack intact BE. In a strain carrying a *ypt1-3* allele, the pre-*HAC1* RNA undergoes diminished exosomal degradation owing to the inability of the mutant protein to recruit NNS/CTEXT/exosome onto this precursor RNA, which in turn facilitates the formation of a pool of precursor *HAC1* mRNAs majority of which carry intact BE . Therefore, This population of pre-*HAC1* RNA with intact BE undergoes more efficient transport from the site of transcription in the nucleus to the Ire1p foci on the ER surface. Collective evidence, therefore, supports the view that Ypt1p dictates the targeting and recruitment of pre-*HAC1* mRNA to Ire1p foci on the ER surface during the activation of UPR, which is accomplished via the recruitment of NNS-CTEXT-exosome onto the *HAC1* pre-mRNA and its subsequent decay.

TABLE 3 Efficiencies of FRET in WT and *ypt1-3* yeast strains (Data associated with Fig. 5C)

FRET efficiencies in WT cells				
Donor-acceptor (*HAC1*^{NRE}-GFP2 + Ire1p-RFP) I_{DA}	Only donor (*HAC1*^{NRE}-GFP2) I_D	Unlabeled sample I_0	FRET efficiency, $E = 1 - \frac{(I_{DA} - I_0)}{(I_D - I_0)}$	Mean FRET WT
571 (Mean, R1)	742 (Mean, R1)	524 (Mean, R1)	0.7251	
517 (Mean, R2)	793 (Mean, R2)	410 (Mean, R2)	0.7206	
621 (Mean, R3)	738 (Mean, R3)	516 (Mean, R3)	0.5270	0.6347
584 (Mean, R4)	768 (Mean, R4)	501 (Mean, R4)	0.6892	
657 (Mean, R5)	785 (Mean, R5)	535 (Mean, R5)	0.5120	
FRET efficiencies in *ypt1-3* cells				
Donor-Acceptor (*HAC1*^{NRE}-GFP2 + Ire1p-RFP) I_{DA}	Only Donor (*HAC1*^{NRE}-GFP2) I_D	Unlabeled sample I_0	FRET efficiency, $E = 1 - \frac{(I_{DA} - I_0)}{(I_D - I_0)}$	Mean FRET *ypt1-3*
658 (Mean, R1)	991 (Mean, R1)	682 (Mean, R1)	1.0776	
662 (Mean, R2)	1194 (Mean, R2)	671 (Mean, R2)	1.0172	
621 (Mean, R3)	897 (Mean, R3)	659 (Mean, R3)	1.1596	1.1032
625 (Mean, R4)	851 (Mean, R4)	665 (Mean, R4)	1.2150	
595 (Mean, R5)	976 (Mean, R5)	612 (Mean, R5)	1.0467	

R: Biological Replicate.

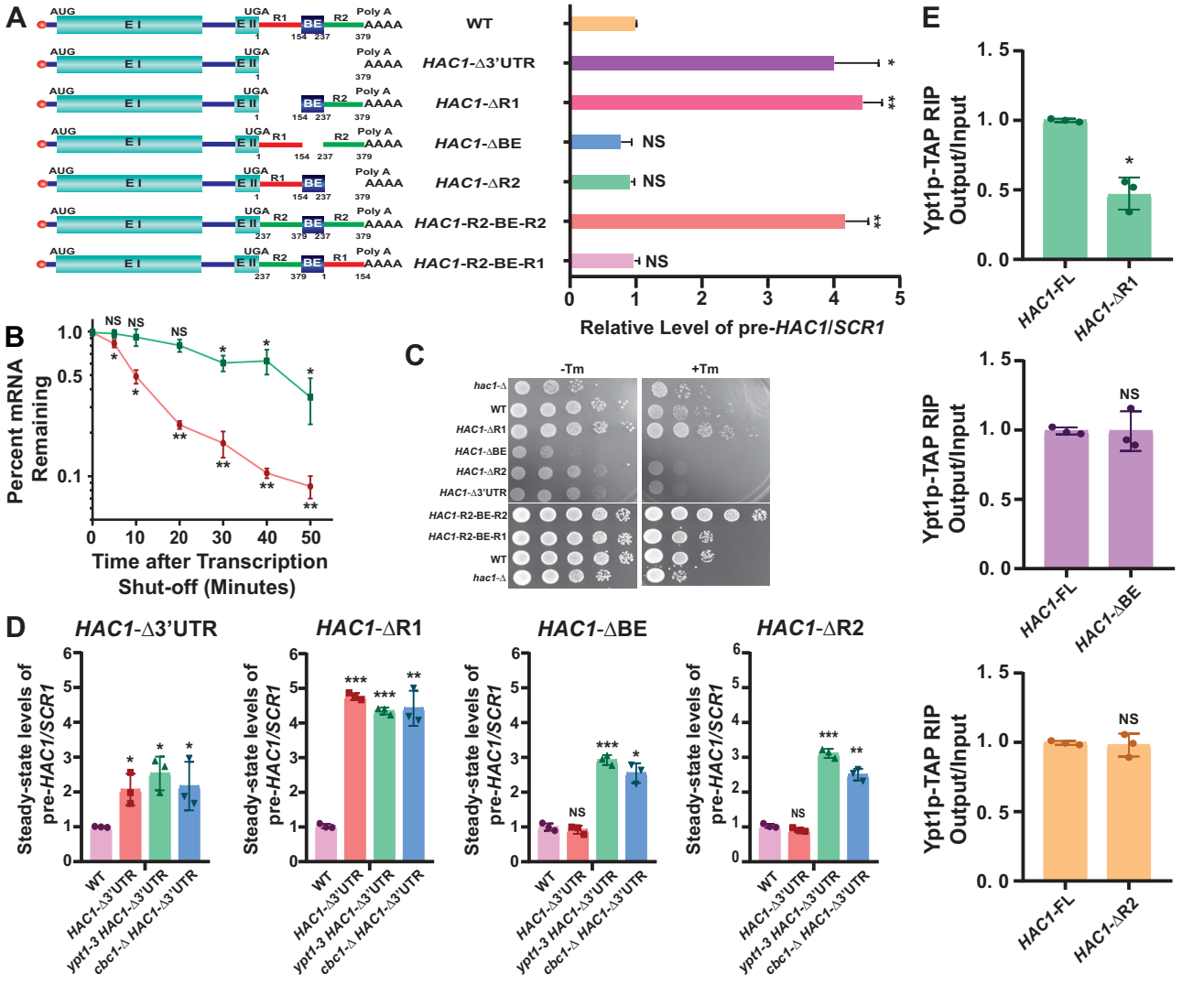

FIG 6 Ypt1p specifically binds to a segment encompassing the first 154 nt of the 3′-UTR of pre-*HAC1* mRNA. (A) Schematic representation of *HAC1* pre-mRNA illustrating its native 3′-UTR and various deletions/manipulations carried out in this region. Relative steady-state levels of full-length *HAC1* pre-mRNA and its various deleted/altered versions as determined by RT-qPCR analysis using a primer set specific to *HAC1* intron. Transcript copy numbers/2 ng cDNA prepared from each strain was normalized to *SCR1* RNA levels obtained from respective strains and the normalized signals are presented as means ± SE (n = 3 for each strain). The normalized value of full-length pre-*HAC1* mRNA was set to one. (B) Decay rates of the full-length pre-*HAC1* (red line) and pre-*HAC1*-ΔR1 (green line) mRNAs as described in Materials and Methods, which were determined from yeast strains expressing either full-length or pre-*HAC1*-ΔR1 deleted version in three independent experiments (biological replicates) by RT-qPCR analysis using the primer sets spanning the *HAC1* intronic sequences (normalized to *SCR1* RNA signals). Normalized signals (mean values ± SD) were presented as the fraction of remaining RNA (with respect to the normalized signal at 0 min) as a function of the time of incubation with transcription inhibitor 1, 10-phenanthroline. C. Relative growth of WT, *hac1*-Δ strains harboring any one of the *HAC1-FL*, *HAC1*-Δ3′-UTR, *HAC1*-ΔR1, *HAC1*-ΔBE, *HAC1*-ΔR2, *HAC1*-R2-BE-R2, and *HAC1*-R2-BE-R1 constructs in YPD solid growth media in the absence (-Tm) and in the presence of 1 μg/mL tunicamycin (+Tm). Equal no. of cells of these yeast strains grown in YPD liquid medium in the absence of tunicamycin was spotted with 10-fold dilution on medium with or without tunicamycin and grown at 30 °C for 72 h and photographed. D. The relative steady-state levels of full-length *HAC1* mRNA and its selected 3′-UTR deleted versions in WT, *ypt1-3*, *cbc1*-Δ strains using RT-qPCR analysis with a primer pair specific to *HAC1* intron. Transcript copy numbers/2 ng cDNA of each strain were normalized to *SCR1* RNA levels in respective strains and are presented as means ± SE (n = 3 for each strain). The normalized value of individual mRNA from normal samples was set to one. The statistical significance of difference as reflected in the ranges of *P* values estimated from Student's two-tailed *t* tests for a given pair of test strains for each message is presented with the following symbols, *<0.05, **<0.005 and ***<0.001, NS, not significant. E. *In-vivo* binding profiles of Ypt1p to the full-length and selected deleted versions of the pre-*HAC1* transcript, which were computed by RT-qPCR following immunoprecipitation by anti-TAP antibody using the whole cell extracts from UV-cross-linked yeast cells expressing TAP-Ypt1p and any one of the pre-*HAC1*, pre-*HAC1*-Δ3′-UTR, pre-*HAC1*-ΔR1, pre-*HAC1*-ΔBE and pre-*HAC1*-ΔR2 transcripts. The mean value from three independent experiments (biological replicates) is shown where immunoprecipitated (output) samples were normalized to input following quantification by real-time PCR. The error bars in the graph represent standard deviations (SD). For A, B, D, and E the statistical significance of difference as reflected in the ranges of *P* values estimated from Student's two-tailed *t* tests for a given pair of test strains for each message are presented with the following symbols, *<0.05, **<0.005, and ***<0.001, NS, not significant.

Ypt1p binds to a specific element located in the 5′-termini of the 3′-UTR of pre-*HAC1* mRNA, which facilitates its degradation by the nuclear decay machinery. Having shown that, the Rab-GTPase Ypt1p plays a pivotal role in the activation

dynamics of UPR signaling, we further query the molecular determinant(s) in *HAC1* pre-mRNA that triggers its susceptibility to nuclear decay factors. A previous study revealed that the 3′-UTR region of the *HAC1* mRNA is necessary for Ypt1-*HAC1* interaction.[32] In determining the putative Ypt1p-binding site in the 3′-UTR of the *HAC1* pre-RNA, we postulated that elimination of the specific segment(s) harboring the Ypt1p-binding site would abolish its rapid exosomal decay leading to a higher steady-state level of the resulting RNA and prevent its participation in UPR response. Consequently, a series of deletion and region-swapped constructs in 3′-UTR of the*HAC1* mRNA was constructed using a combination of restriction endonuclease-digestion and reverse PCR technology (Fig. 6A, left cartoon). Comparison of the steady-state levels of the full-length pre-*HAC1* transcript and its various deleted versions in the absence of ER stress revealed that the levels of *HAC1*-ΔR2 and *HAC1*-ΔBE mRNAs are low and similar to the physiological level of full-length message (Fig. 6A, right histogram). The abundance of *HAC1*-Δ3′-UTR and *HAC1*-ΔR1, in contrast, increased by 4 and 4.5-fold, respectively, relative to the full-length message (Fig. 6A, right histogram). This data suggest that the region 1 (R1) spanning 1 to 154 nt residues of the 3′-UTR of the pre-*HAC1* mRNA (Fig. 6A, left cartoon) plays a vital role in governing the stability of this RNA and in dictating its susceptibility to the CTEXT/nuclear exosome. To query if Ypt1p binding to pre-*HAC1* mRNA requires the mere length of the 3′-UTR rather than any specific sequence, we evaluated the relative level of pre-*HAC1* message from a construct that carries two copies of region 2 (R2) flanking the BE element (*HAC1*-R2-BE-R2, Fig. 6A left cartoon). Although, the resulting R2-BE-R2 3′-UTR is shorter by only 12 nucleotides (nt) (367 nucleotides) than native R1-BE-R2 3′-UTR (379 nucleotides) it did not support the decay of this precursor RNA as evident from the significantly higher steady-state level of the resulting precursor transcript (Fig. 6A, right histogram). Remarkably, mutual swapping of the R1 and R2 creating R2-BE-R1 3′-UTR led to the abundance of the resulting RNA to the level that is comparable to the level of native *HAC1*-3′-UTR, and *HAC1*-ΔR2 pre-RNAs (Fig. 6A, right histogram). These data suggest that the presence of region 1 (R1) in the pre-*HAC1* mRNA is extremely vital for the binding of Ypt1p and subsequent targeting of this precursor RNA to the NNS/CTEXT/exosome complex. It appears that as long as the R1 element is placed at any position within the 3′-UTR, it permits Ypt1p binding and its context appears to be less important (Fig. 6A, right histogram). Collective data therefore suggests that the presence of the R1 element anywhere in the pre-*HAC1* mRNA 3′-UTR promotes its exosomal degradation, whereas its elimination from the pre-*HAC1* transcript abolished its susceptibility to the nuclear exosome and CTEXT, which is caused by the exclusion of the putative Ypt1p binding site from this precursor mRNA.

To establish whether the higher abundance of the *HAC1*-ΔR1 transcript is accompanied by its diminished decay rate, we analyzed the decay rates of full-length *HAC1* and *HAC1*-ΔR1 transcripts in the WT strain expressing functional Ypt1p. As shown in Fig. 6B, the decay rate of the *HAC1*-ΔR1 mRNA was found to diminish substantially relative to that of the full-length *HAC1* thereby suggesting that elimination of the R1 region indeed lowered its susceptibility to the nuclear exosome/CTEXT and increased the stability of the pre-*HAC1* mRNA. Consistently, when yeast strains expressing the full-length and various deleted versions of *HAC1* pre-mRNA were challenged with tunicamycin, the strain harboring the pre-*HAC1*-ΔR1 and *HAC1*-R2-BE-R2 alleles exhibited higher survival and resistance to the ER-stress (Fig. 6C).

Next, we validated the functional role of the putative Ypt1p-binding element on the decay of pre-*HAC1* message by additionally investigating the effect of mutations in *YPT1* (*ypt1-3*) and *CBC1* (*cbc1-Δ*) genes on the abundance of full-length and various deleted versions of pre-*HAC1* mRNAs. As shown in Fig. 6D, the steady-state levels of *HAC1*-ΔBE and *HAC1*-ΔR2 mRNAs were enhanced in strains expressing these *HAC1* alleles and additionally carrying either *ypt1-3* or *cbc1-Δ* alleles relative to either isogenic WT or *HAC1*-ΔBE/*HAC1*-ΔR2 strains (Fig. 6D). The abundance of the *HAC1*-Δ3′-UTR and *HAC1*-ΔR1 messages, however, did not display any further enhancement in

the *ypt1-3* and *cbc1*-Δ mutant yeast strains relative to their isogenic *HAC1*-Δ3′-UTR/*HAC1*-ΔR1 strains (Fig. 6D). This finding indicates that both *HAC1*-ΔR1 and *HAC1*-Δ3′-UTR mRNAs lacking the Ypt1p binding element failed to recruit the nuclear decay machinery in the absence of ER stress leading to their diminished degradation and thus mutations in the *YPT1/CBC1* gene did not have any further effects on their stability (Fig. 6D). In contrast, *HAC1*-ΔBE and *HAC1*-ΔR2 messages still harboring the Ypt1p-binding site underwent a rapid Ypt1p-dependent degradation in the nucleus in the absence of ER stress and displayed an increase in their steady-state levels in *ypt1-3* and *cbc1*-Δ mutant backgrounds. Collective data thus suggest that the Ypt1p-binding element is present within the first 154 base pair (bp) region of *HAC1* 3′-UTR, which is responsible for its exosome/CTEXT-dependent nuclear decay.

Next, we investigated the binding of the Ypt1p to the full-length and diverse deleted versions of the pre-*HAC1* mRNAs *in vivo* using RNA immunoprecipitation (RIP). RIP signals were estimated from the extract prepared from yeast strains expressing TAP-Ypt1p and either a full-length (FL) or a deleted version of the pre-*HAC1* mRNA (Fig. 6E). As shown in Fig. 6E, a significantly lower RIP signal was noted in *HAC1*-ΔR1 transcripts lacking the Ypt1p binding-site relative to full-length (FL) RNA, whereas a similar and comparable RIP-signal were observed for both of the *HAC1*-ΔR2 and *HAC1*-ΔBE mRNAs, affirming that these mutant versions still harbor the Ypt1p binding site.

To strengthen the above finding, we subjected the R1 segment of the pre-*HAC1* 3′-UTR harboring the Ypt1p-binding element to two different kinds of *in vitro* binding assays (i) a StreptoTag-based affinity purification system[38] and (ii) electrophoretic mobility shift assay (EMSA) to inquire if the Ypt1p binds this RNA element *in vitro*. For StreptoTag affinity purification assay, four different RNA sequences corresponding to entire *HAC1* 3′-UTR, regions R1, BE and R2 were separately fused to a StreptoTag aptamer by two independent PCR reactions using a cloned version of *HAC1* gene as a template as illustrated in Fig. 7A for region R1. These reactions employed a sense primer harboring a T7 promoter fused in tandem to 5′-segment of any of the 3′-UTR, R1, BE, or R2 regions and an antisense primer carrying the 3′-segments of any of the 3′-UTR, R1, BE, or R2 regions fused in tandem to full-length StreptoTag aptamer sequence (Fig. 7A). The amplified products from each of these reactions were further used as the templates for separate *in vitro* transcription reactions using T7 RNA polymerase (Fig. 7A). The resulting fusion RNAs consisting of any of the 3′-UTR, R1, BE, or R2 sequence fused to StreptoTag aptamer in tandem (Fig. 7A) were subjected to two independent coupling reactions to epoxy-activated Sepharose 6B resin in the presence of 1 mM dihydrostreptomycin (Fig. 7B). One mg of total protein extract from strain expressing TAP-Ypt1p were mixed separately with any of the immobilized RNA-streptoTag sequences (3′-UTR-streptoTag, R1-streptoTag, BE-streptoTag or R2-streptoTag) aptamer complexes in Sepharose 6B column (Fig. 7B). The columns were washed with tRNA and finally, the bound RNA-protein complexes were eluted with streptomycin (Fig. 7B). The input and the two eluate samples from each column were subjected to Western blot analysis using an anti-TAP antibody (Ypt1p N-terminally TAP-tagged). As shown in Fig. 7C, Ypt1p was detected in both the input and eluate samples containing either the154 nt sequence corresponding to the R1 region or the 379 nt sequence containing the entire 3′-UTR sequence both of which harboring the Ypt1p binding site as the bait. No Ypt1p was detected in the second eluate sample that contained either the 83 nt BE region or 142 nt R2 as the bait (Fig. 7C). Furthermore, in another independent experiment, separate protein extracts prepared from yeast strains expressing either functional Ypt1p or mutant Ypt1-3p were also subjected to StreptoTag affinity purification with R1-streptoTag as a bait. As shown in Fig. 7C, no signal was detected in the extract prepared from the strain expressing the mutant protein. Data from these experiments confirmed that Ypt1p indeed binds to the 154 nt *cis*-acting element corresponding to the region 1 (R1) either as an isolated element or as a part of the 3′-UTR sequence of pre-*HAC1* mRNA.

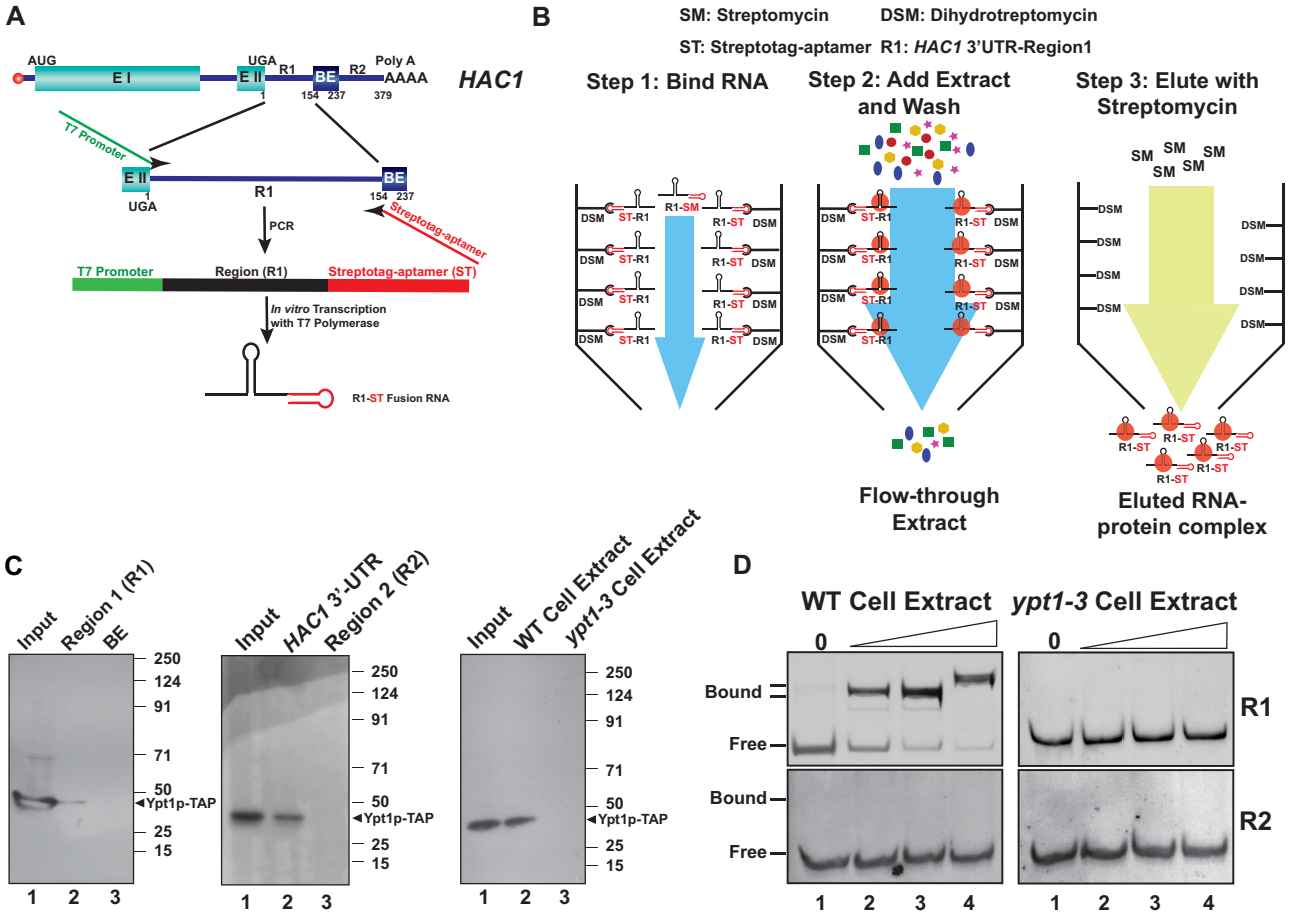

FIG 7 Ypt1p specifically binds to the region 1 (R1) of 3′-UTR of pre-*HAC1* mRNA *in vitro*. (A) Cartoon showing the strategy to prepare *HAC1*-R1/R2/BE/3′-UTR-StreptoTag (R1-ST, R2-ST, BE-ST, etc.) aptamer fusion RNA. A cloned version of the *HAC1* gene was subjected to a PCR reaction using a set of overhang primer sets. The primer sets consist of a forward primer harboring T7 promoter sequence (green line) and a sequence complementary to the 5′-end of the Region R1/R2/BE etc. (black right arrowhead) and a reverse primer carrying StreptoTag aptamer sequence (red line) and a sequence complementary to the 3′-end of the Region R1/R2/BE etc. (black left arrowhead). The resulting linear PCR product harboring sequences of T7 promoter (green), Region R1/R2/BE, etc. (black), and StreptoTag aptamer (red) in tandem was used for *in vitro* transcription using T7 RNA polymerase to produce copious amounts of R1/R2/BE-ST fusion RNA that was bound to the dihydrostreptomycin coupled to epoxy-activated Sephadex-6B. (B) Cartoon representing the rationale of the StreptoTag affinity purification procedure. The bait R1/R2/BE-ST fusion RNAs bound dihydrostreptomycin (DSM) was coupled to epoxy-activated Sephadex-6B followed by the addition of the appropriate yeast cell extracts for binding/immobilization of the prey protein(s). After repeated washing, the bound RNA protein complex was eluted with streptomycin (SM, having a higher affinity to StreptoTag aptamer than dihydrostreptomycin, DSM). (C) StreptoTag affinity purification profile showing that functional TAP-Ypt1p selectively binds to the Region 1 (R1) of *HAC1* 3′-UTR. Left and middle panels, Protein extract prepared from WT yeast cells expressing TAP-Ypt1p was subjected to four separate StreptoTag affinity purification procedures using any one of *HAC1*-R1 (R1-StreptoTag), *HAC1*-BE (BE-StreptoTag), *HAC1*-3′-UTR (UTR-StreptoTag), *HAC1*-R2 (R2-StreptoTag) segments as bait followed by elution from the column and immunoblotting with anti-TAP antibody. Right panel, same as left and middle panels except the bait used in this experiment was *HAC1*-R1 (R1-StreptoTag) and the protein extracts were prepared either from WT cells expressing TAP-Ypt1p or from a mutant strain expressing TAP-Ypt1-3p. Eluates from individual purification were subjected to Western blot analysis using anti-TAP antibody. (D) Electrophoretic mobility shift analysis showing that WT functional TAP-Ypt1p selectively binds to the Region 1 (R1) of *HAC1* 3′-UTR. 65 μg of purified Region 1 (R1)/2 (R2) RNA prepared by *in vitro* transcription was subjected to *in vitro* binding reaction using the 0, 5, 10, and 20 μg cell extracts prepared either from WT (*YPT1*) or from mutant (*ypt1-3*) yeast strains as described in Materials and Methods followed by native polyacrylamide gel electrophoresis.

To corroborate further the binding of Ypt1p with the R1 sequence using another independent technique, we subjected the cell extracts prepared from either WT or mutant *ypt1-3* yeast strains to either purified R1 or purified R2 RNA sequences in an RNA-EMSA. As shown in Fig. 7D, a distinct shift in the mobility of only the R1 sequence was observed when increasing concentrations of cell extract from the WT yeast strain was used in the experiment. Interestingly, a super-shifted band of protein bound R1 element was noted when the highest concentration (20 μg of total protein) cell extract was used in the binding reaction (Fig. 7D, lane 4 in top right panel). However, since crude cell extract was used in this assay it is difficult to conclude if this super-shifted band has any physiological significance. Notably, no shift in the mobility of either the

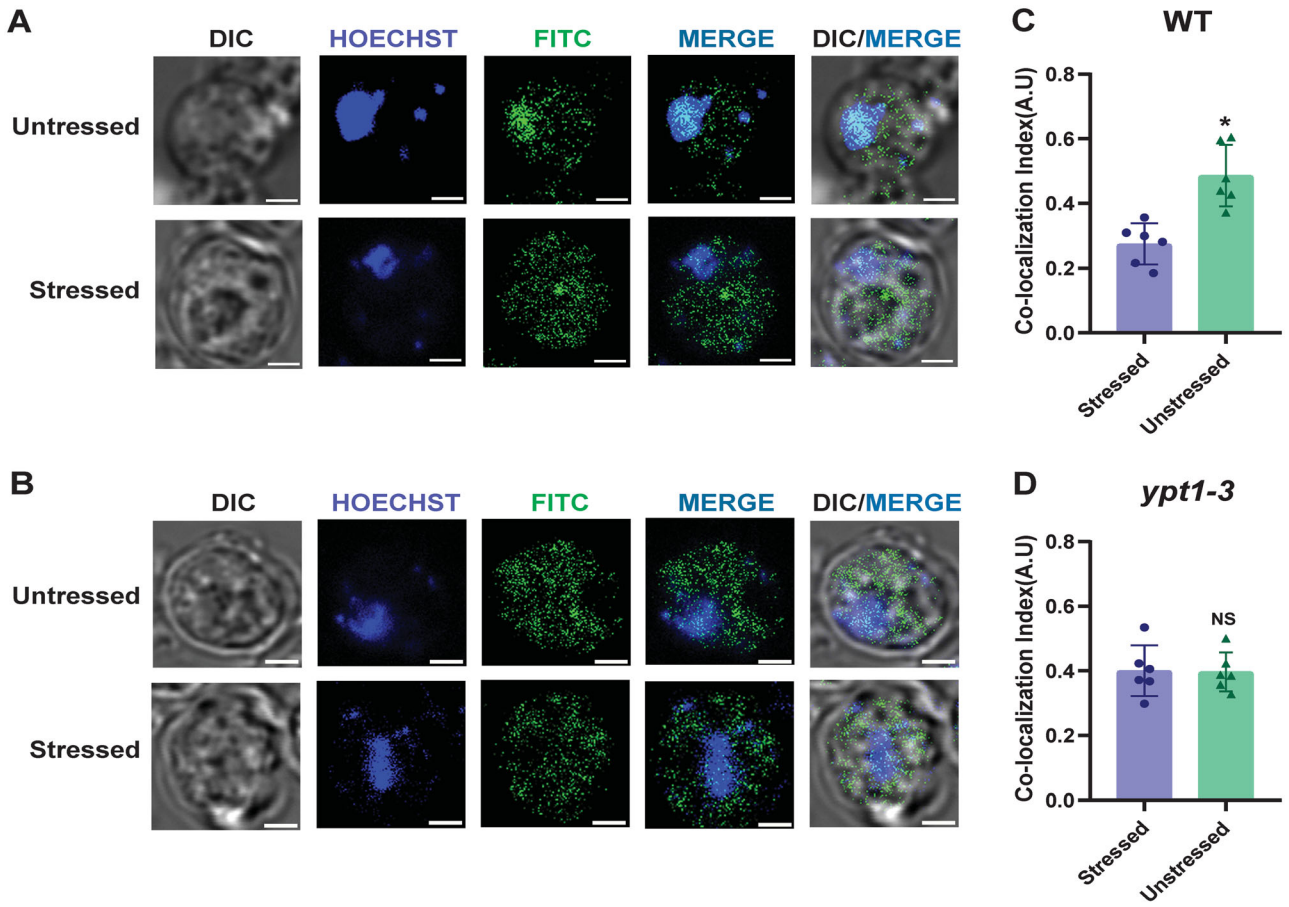

FIG 8 Part of Cellular Ypt1p pool distributes in the nucleus in the absence of ER stress, which relocalizes to the cytoplasm during the ER stress. (A and B) Localization of N-terminally TAP-tagged WT Ypt1p (A) and mutant Ypt1-3p (B) expressed from their native promoters as determined by immunofluorescence using rabbit anti-TAP primary antibody followed by anti-rabbit FITC conjugated secondary antibody in both unstressed (upper panel) and ER-stressed (induced by 1 μg/mL tunicamycin for 30 min) (lower panel) condition. The nucleus of both samples was stained with Hoechst stain. The white bar in each image panel indicates two micrometers. (C and D) Histogram depicting the colocalization of either WT Ypt1p FITC signal/Hoechst (nucleus) (C) or mutant Ytp1-3p FITC signal/Hoechst (nucleus) (D) before and after ER stress was induced. Colocalization indices (Pearson's correlation coefficient, PCC) were expressed in arbitrary units and were determined as described in the Materials and Methods section. Colocalization data for this figure are presented in Table 8. The statistical significance of difference as reflected in the ranges of *P* values estimated from Student's two-tailed t-tests for a given pair of test strains for different conditions are presented with the following symbols, *$<$0.05, **$<$0.005 and ***$<$0.001, NS, not significant.

R1 fragment was noted when extract from mutant *ypt1-3* yeast strain was used (Fig. 7D). Moreover, the R2 fragment did not display any shift in the mobility when the extract from either WT strain or from mutant *ypt1-3* strain was used in this assay (Fig. 7D). Collective findings thus revealed that Ypt1p binds to the pre-*HAC1* message in a region spanning the residues 1–154 of its 3′-UTR, which in turn further recruits NNS, CTEXT, and exosome complex, thereby promoting the rapid decay of this precursor RNA.

A fraction of cellular Ypt1p localizes to the nucleus in the absence of ER stress, which redistributes to the cytoplasm when ER stress is imposed. Next, we investigated the cellular distribution of Rab-GTPase Ypt1p in both ER-stressed and unstressed conditions to determine whether Ypt1p at all localizes to the nucleus. The protein was expressed from its native promoter as N-terminally TAP-tagged fusion and its intracellular localization was observed by indirect immunofluorescence followed by confocal imaging. As shown in Fig. 8A, in the unstressed condition while the majority of Ypt1p displays cytoplasmic localization, a certain fraction of it was indeed found to localize into the nucleus (stained by Hoechst stain) (Fig. 8A). In contrast, under ER-stressed condition, most of the nuclear Ypt1p pool appears to exclude from the nucleus by redistributing to the cytoplasmic territory in all visible fields (Fig. 8A). Analysis of the colocalization index between the Hoechst (nucleus) and the Ypt1p-FITC signals

TABLE 4 Colocalization index of FITC (TAP-Ypt1p or TAP-Ypt1-3p) and Hoechst (nucleus) in WT strains in unstressed and ER stressed WT and mutant *ypt1-3* yeast strain (Data associated with Fig. 8C and D)

Replicates	WT TAP-Ypt1p		MutantTAP-Ypt1-3p	
	Stressed	Unstressed	Stressed	Unstressed
1	0.185 (Mean, R1)	0.4778 (Mean, R1)	0.4056 (Mean, R1)	0.4232 (Mean, R1)
2	0.2996 (Mean, R2)	0.6048 (Mean, R2)	0.3714 (Mean, R2)	0.3849 (Mean, R2)
3	0.2817 (Mean, R3)	0.427 (Mean, R3)	0.2985 (Mean, R3)	0.3567 (Mean, R3)
4	0.3096 (Mean, R4)	0.4391 (Mean, R4)	0.4231 (Mean, R4)	0.3876 (Mean, R4)
5	0.3564 (Mean, R5)	0.3718 (Mean, R5)	0.3678 (Mean, R5)	0.3276 (Mean, R5)
6	0.2165 (Mean, R6)	0.5956 (Mean, R6)	0.5346 (Mean, R6)	0.5005 (Mean, R6)
Mean	0.2748	0.4860	0.4002	0.3968

R: biological replicate.

revealed a significantly (2-fold) higher colocalization index during the unstressed condition that was drastically reduced when ER-stress was imposed (Fig. 8C) (colocalization data of this experiment is provided in Table 4). Interestingly, unlike the WT Ypt1p, the mutant Ypt1-3p protein did not display a significant amount of nuclear localization either in stressed or unstressed conditions (Fig. 8B), which was consistently reflected in its colocalization index during both conditions (Fig. 8D) (Colocalization data of this experiment is provided in Table 4). This interesting finding, therefore, suggests that in the absence of ER stress, a finite fraction of the cellular Ypt1p pool localizes to the nucleus (Fig. 8A, top merge panel), and undergoes cotranscriptional recruitment onto the pre-*HAC1* message. ER stress promotes a rapid redistribution of the nuclear Ypt1p pool to cytoplasm leading to its significant exclusion from the nuclear territory (Fig. 8A, bottom merge panel) causing its inability to bind to the *HAC1* precursor RNA. The majority of the mutant Ypt1-3p was unable to localize to the nucleus (Fig. 8B) and failed to bind to the pre-*HAC1* message (Fig. 7C), which in turn led to its failure to promote the nuclear decay of this precursor RNA. Reversible nuclear localization of a fraction of cellular Ypt1p pool during the unstressed condition, thus, provides a mechanism, which may regulate the Ypt1p-association with pre-*HAC1* mRNA during UPR signaling dynamics in baker's yeast.

DISCUSSION

Diverse extracellular insults and aberrations in protein folding result in a disparity in the normal protein folding activity of ER thereby leading to the accumulation of misfolded proteins in the ER lumen, dubbed "ER stress". The unfolded protein response (UPR) readjusts ER folding capacity to restore protein homeostasis within ER lumen. The key transcription activator involved in UPR, Hac1p responds to ER stress by activating the genes encoding ER chaperones, which collectively refold the unfolded ER proteins and thereby restore ER homeostasis. The efficiency of the delivery and recruitment of the precursor *HAC1* mRNA from the nuclear territory to the Ire1p foci on the ER surface is governed by the bipartite element (BE) present in the 3′-UTR of this mRNA for its successful nonspliceosomal splicing.[29] Remarkably, reversible and dynamic nuclear decay of this precursor message dependent on the nuclear exosome and CTEXT dictates the effective cellular concentration of recruitment-competent *HAC1* pre-mRNA that harbors the BE element.[31] Preferential nuclear mRNA degradation of this precursor RNA thus plays a pivotal role in tuning the gain of the UPR signaling dynamics.[31] Nevertheless, the precise mechanism of specific and selective recognition of *HAC1* pre-mRNA from the vast majority of other nuclear messages by the nuclear decay machinery remained obscure. Evidence of the association of the Rab-GTPase Ypt1p to unspliced *HAC1* message leading to alteration of its stability[32] inspired us to explore if Ypt1p plays any role in the recognition and targeting of the *HAC1* pre-mRNA.

Employing the mutant *ypt1-3* allele, we established that indeed Ypt1p plays an important role in controlling the UPR signaling dynamics in *S. cerevisiae*, which was based on the findings that (i) the mutant *ypt1-3* strain displayed better growth/survival

pattern under ER stress at 30 °C and improved resistance to stress relative to a normal WT strain (Fig. 2A to C). It is noteworthy here that although the yeast strain carrying a conditional *ypt1-3* allele exhibits a clean temperature sensitive phenotype concerning its growth[39] (Fig. 2), this allele does not always confer a clean temperature-dependent phenotype concerning other traits. For example, the ability of *ypt1-3* strain (i) to secrete invertase[39] and (ii) to participate in nonspecific autophagy[40] are perfectly normal at the permissive temperature of 25 °C and are dramatically affected at the conditional temperature of 37 °C. However, the ability of the mutant *ypt1-3* strain to take part in the specific autophagy via the Cvt pathway[40] is not significantly compromised at 37 °C. Unlike the WT allele, the mutant *ypt1-3* ts allele exhibits a partial ability to hydrolyze a precursor amino-peptidase at both 25 °C and 37 °C thereby indicating that the mutant protein does not retain its function at the permissive condition of 25 °C.[40] Interestingly, the data from our experiments involving the growth and survival profiles of this mutant strain (Fig. 2) indeed suggest that even at the permissive and semirestrictive temperatures of 25 °C and 30 °C, the mutant Ypt1-3p exhibits a mild and strong phenotype of controlling the UPR signaling dynamics respectively. This observation suggests that the mutant protein does not preserve the majority of its function at 30 °C concerning its ability to undergo cotranscriptional recruitment onto pre-*HAC1* mRNA. A significant loss of function phenotype of the *ypt1-3* allele at 30 °C and its inability to grow and survive at the conditional temperature of 37 °C, therefore, prompted us to select the semirestrictive temperature of 30 °C at which the experiments involved in comparative protein-protein and RNA protein binding with the functional and mutant Ypt1p proteins were carried out.

Notably, growth and survival profiles exhibited by the *nrd1-1* and *ypt1-3* alleles at 30 °C in the absence and in the presence of ER-stress show a very similar phenotype shown by the previously characterized yeast mutants deficient in the nuclear mRNA decay (such as exosome deficient *rrp6*-Δ and CTEXT deficient *cbc1*-Δ yeast strains).[31] All the mutants having defects in the genes encoding components of the nuclear decay machinery (*YPT1*, *NRD1*, *CBC1,* and *RRP6*) exhibit an enhanced survival ability in the presence of ER stress and increased resistance to these stressors. This finding may appear puzzling since the regulatory circuit involving the nuclear mRNA decay imparts an additional sensitivity in the WT cells to ER stress relative to the mutant cells defective in mRNA decay since they exhibit increased resistance to ER stressors. This apparent paradox is resolved by the argument that the regulatory circuit involving mRNA decay and targeting provides a fine regulation of the levels of pre-*HAC1* message involving a preferential mRNA decay. Regulated degradation of the pre-*HAC1* message by the nuclear exosome/CTEXT finely tunes the UPR signaling dynamics in a reversible manner that is also necessary to attenuate the UPR signaling via reinstating the rapid nuclear mRNA decay once ER homeostasis is restored.

The resemblance in the growth/survival phenotypes of all the mRNA decay mutants in the presence of ER stress indicates that Ypt1p and Nrd1p participate in the same Cbc1p/Rrp6p-dependent nuclear decay pathway that controls the UPR signaling dynamics via the rapid decay of pre-*HAC1* RNA. Our data demonstrated that in the absence of ER stress, Ypt1p functions in the initial recognition of pre-*HAC1* mRNA, which is preceded by the sequential recruitments of Nrd1p (the NNS), the CTEXT, and the nuclear exosome onto pre-*HAC1* mRNA thereby promoting its nuclear decay. Thus, Ypt1p plays a crucial role in the initial "marking" of the precursor *HAC1* mRNA and further coordinating the sequential recruitments of NNS, exosome, and CTEXT components onto this RNA (Fig. 1 to Fig. 4). Collective data from all these experiments argue in favor of a model that Ypt1p initially recognizes the pre-*HAC1* mRNA and further promotes the cotranscriptional recruitment of the NNS complex, the CTEXT, and the nuclear exosome onto it in a sequential manner to trigger its preferential nuclear decay (Fig. 9). Preferential recruitment of Ypt1p onto pre-*HAC1* mRNA thus provides a key mechanism by which this precursor message is initially recognized by the decay

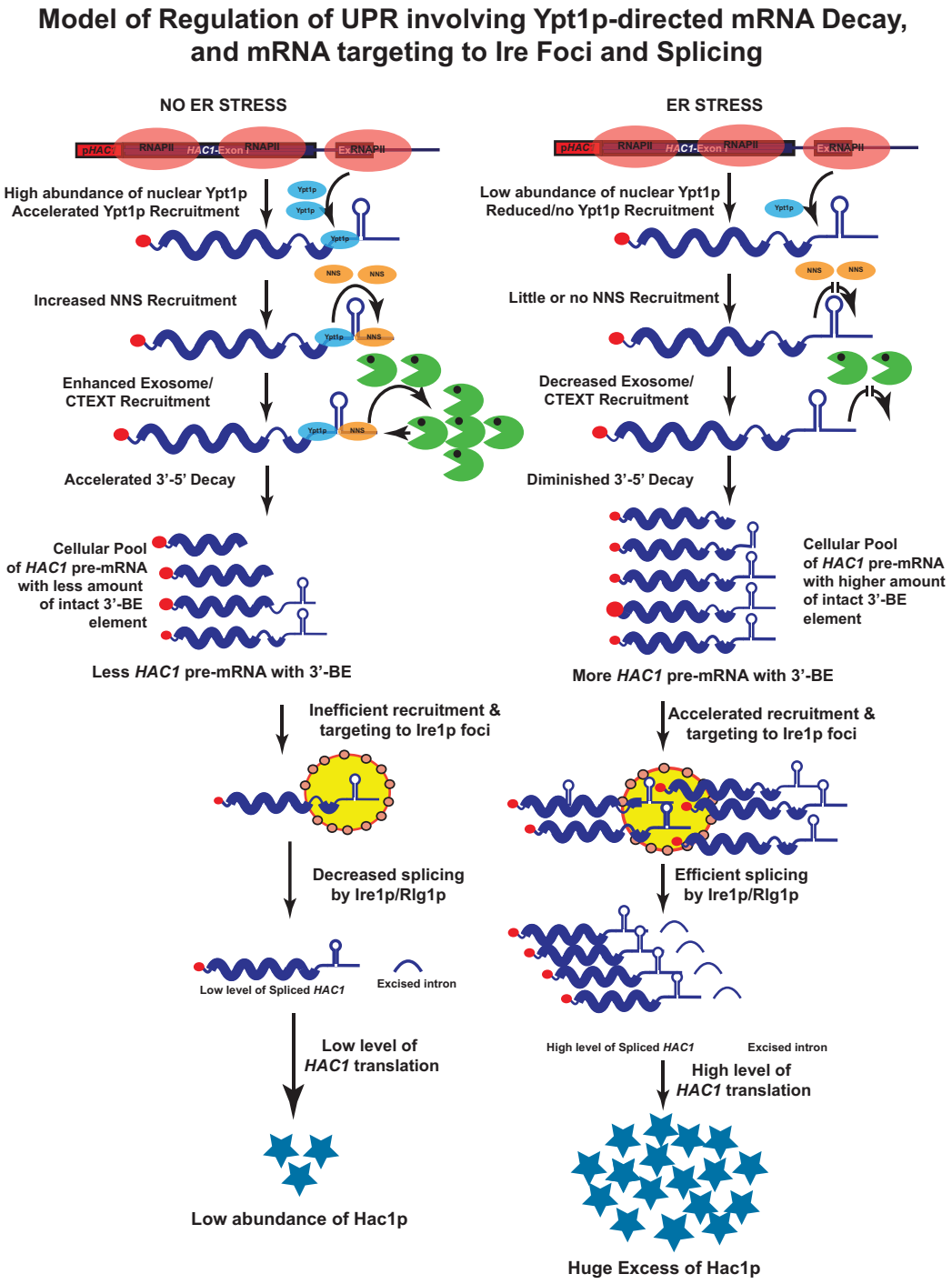

FIG 9 Model of Ypt1p-directed regulation of UPR in baker's yeast. Left side. In the absence of ER stress, nuclear Ypt1p is co-transcriptionally recruited on to precursor *HAC1* message in a selective fashion that further promotes the sequential cotranscriptional recruitment of NNS, CTEXT, and the nuclear exosome onto this precursor message and triggers its dynamic and reversible 3′→5′ degradation. This rapid decay results in the formation of a *HAC1* precursor RNA pool most of which lack the intact BE leading to their less efficient delivery to Ire1p foci, less splicing, and translation. Right side. ER-stress triggers the relocalization of Ypt1p from the nucleus to cytoplasm leading to its inefficient recruitment onto the precursor *HAC1*, which in turn affects the loading of the decay factors on this precursor RNA resulting in its diminished decay. Diminished pre-*HAC1* decay leads to the formation of a pool of *HAC1* pre-RNA with an intact and functional BE, which are targeted and recruited more efficiently to the Ire1p foci leading to more efficient splicing and translation.

machinery in a selective fashion from the vast majority of normal and other aberrant messages.

Consistent with the characteristic directionality of the exosomal degradation of pre-*HAC1* mRNA that typically initiates from the extreme 3′-termini of the precursor

message, our data suggest that Ypt1p binds to the region 1 (R1) (encompassing 1–154 nt relative to TGA codon) of the 3′-UTR of pre-*HAC1* mRNA. Interestingly, Ypt1p binds to the R1 region *in vivo* (using the RIP technique) (Fig. 6E) as well as in vitro (using the StreptoTag affinity purification system and electrophoretic mobility shift assay) (Fig. 7C and D). Importantly, neither the mutant Ypt1-3p protein displayed any binding to the R1 region in both in vivo and in vitro binding assays nor did the functional Ypt1p protein show any affinity to BE and R2 regions in our StreptoTag procedure. Moreover, the stability of the two of the altered versions of *HAC1* pre-RNA, the *HAC1*-ΔR1 and *HAC1*-R2-BE-R2, both of which lacked the region 1 (R1) displayed much higher stability relative to the full-length *HAC1* precursor in the WT yeast strain equipped with functional NNS complex and nuclear decay machinery (Fig. 6A). Collective data, therefore, affirmed that the binding of Ypt1p to the region R1 is extremely specific and physiologically relevant. Once Ypt1p binds to the region R1 in the absence of ER-stress, it further recruits the NNS complex presumably in the close vicinity of the *HAC1* pre-mRNA transcript body, which in turn assists loading of the nuclear exosome and CTEXT presumably at the extreme 3′-termini to promote its nuclear decay (Fig. 9).

In agreement with the nuclear role of Ypt1p, our data suggests that it is a shuttling protein. In the absence of ER stress, while a substantial amount of cellular Ypt1p localizes to the cytoplasm, a finite fraction of this pool also distributes in the nucleus that preferentially undergoes cotranscriptional recruitment onto *HAC1* precursor RNA. Upon imposition of ER stress, part of this nuclear pool quickly redistributes to the cytosol (Fig. 8). Although the mechanism of reversible binding of Ypt1p to the pre-*HAC1* mRNA during various phases of ER-stress is currently obscure, the reversible nucleocytoplasmic shuttling of a fraction of cellular Ypt1p during various phases of the UPR provides a possible means by which this regulation is accomplished. Notably, Ypt1p lacks a classical nuclear localization signal (NLS) that is typically recognized by importin α/β and RAN-GTPase, which play a major role in importing various cargo proteins from cytosol into the nucleus.[41] Remarkably, Ypt1p was demonstrated to interact with Ada5p/Spt20 in the absence of ER stress,[32] a component of the SAGA histone acetylation complex involved in transcriptional activation.[42] Ada5p/Spt20p is known to localize in the nucleus using its nuclear localization signal (spans 562–591 aa residues of Ada5p primary sequence). Although the actual mechanism of nuclear import of Ypt1p is unknown, it will not be unreasonable to speculate that Ada5p via its interaction with Ypt1p may carry Ypt1p to the nucleus in a passive manner. In this context, it would be relevant to discuss that despite being a membrane protein, the UPR transducer Ire1p harbors a classical nuclear localization signal,[43] and this protein was demonstrated to shuttle into the nucleus in a RAN-GTPase/Importin β-dependent manner.[43] Remarkably, a mutation in the Ire1p NLS abolishes UPR in yeast[43] thereby suggesting that Ire1p nuclear shuttling is a vital event that plays an instrumental role in the proper execution of the UPR. Although Ire1p-nuclear shuttling and its actual connection to UPR signaling is yet an unexplored area, it would be exciting to invoke that perhaps the pre-*HAC1* mRNA may be targeted to the nuclear fraction of Ire1p and this pre-*HAC1* bound nuclear Ire1p comes back to the ER from the nucleus by an unknown mechanism for oligomerization and subsequent splicing. Future research addressing the mechanism of nuclear shuttling of Ypt1p and Ire1p during various phases of UPR and their connections to the other regulatory events will throw light on the unexplored phase of the regulatory circuit of this important signaling pathway.

The existence of a separate layer of regulation in the control of cellular UPR signaling dynamics suggests a possible mechanism by which a small extent of signaling cue can amplify the final output of this pathway optimally. It is noteworthy that protein-unfolding status within the ER lumen may be sensed by two different sensors, which are eventually transduced into the massive production of Hac1p (Fig. 10). While one sensor of protein unfolding is Ire1p, the other sensor is probably Ypt1p. As reported by numerous laboratories, the sensing of the unfolding status by Ire1p is

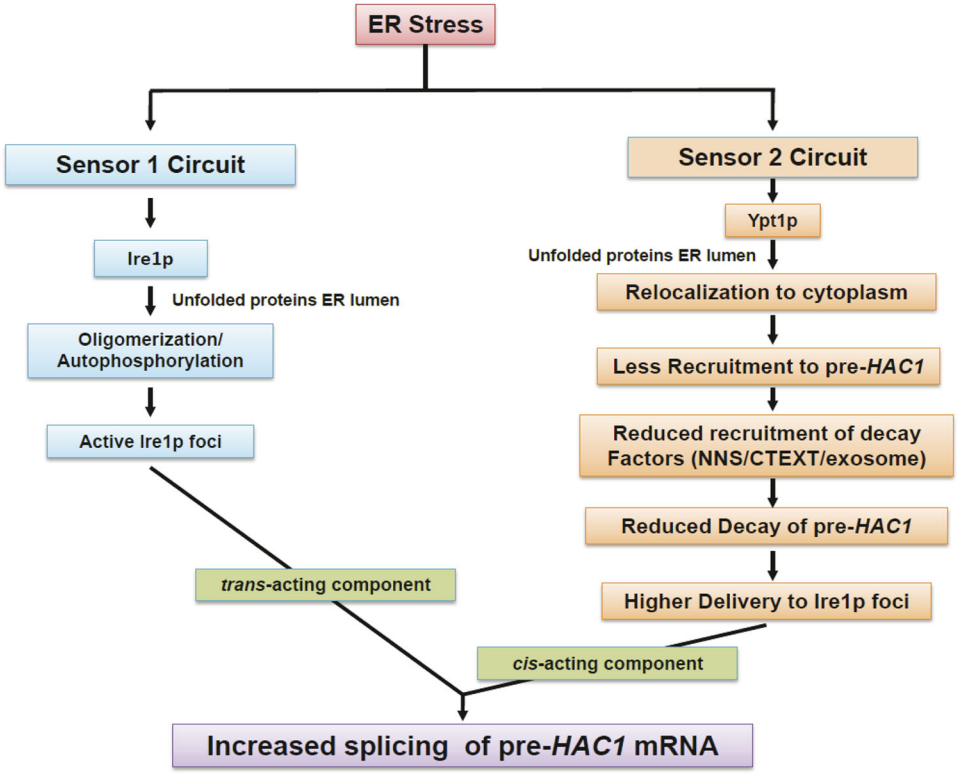

FIG 10 Two independent regulatory circuits control of activation of UPR signaling dynamics in baker's yeast. Cartoon depicting two different sensors that sense the unfolded proteins within the ER lumen during the activation stage of UPR. While Ire1p serves as one of the sensors, Ypt1p plays a crucial role as the other sensor. Sensing by Ire1p is characterized by its oligomerization and formation of an active RNase domain that eventually splices out the *HAC1* intron. Sensing by Ypt1p, in contrast, is accompanied by its quick relocalization from the nucleus to the cytoplasm thereby causing its decreased recruitment onto pre-*HAC1* mRNA resulting in its diminished decay and increased delivery to Ire1p foci. The timely convergence of the output signals from two independent circuits on the Ire1p interface on ER surface during the activation phase of ER stress results in an amplified integrated signal that eventually produces copious amounts of functional mature *HAC1* mRNA and Hac1p protein.

followed by its oligomerization leading to the activation of its RNase domain that eventually splices out the *HAC1* intron.[27,28,44,45] Sensing by Ypt1p, in contrast, is manifested by its quick relocalization from the nucleus to the cytoplasm thereby causing its decreased recruitment onto pre-*HAC1* mRNA resulting in its diminished nuclear decay and increased delivery to Ire1p foci (Fig. 10). The discovery of this second regulatory circuit involving nuclear mRNA decay that functions upstream of the Ire1p sensing circuit is a unique characteristic of this signaling mechanism. The existence of the two independent circuits enables their outputs to converge on the Ire1p interface on ER surface during the imposition of ER stress thereby magnifying the final transduced output in a synergistic fashion (Fig. 10). Ypt1p thus plays a vital role in sensing the ER-stress signal independently and transduce that signal to the Ire1p kinase-endoribonuclease (*trans*-acting component) via the increased delivery of pre-*HAC1* mRNA (*cis*-acting component) during the activation phase of UPR.

MATERIALS AND METHODS

Strains, plasmids, and oligonucleotides. The genotypes of *S. cerevisiae* strains used in this study are listed in Table 5. Yeast genetic analysis was carried out by standard procedures.[46] The plasmids were either procured from other laboratories or were constructed in this laboratory using standard procedures. All the oligonucleotides were obtained commercially from Integrated DNA Technology (Coralville, IA, USA). The plasmids and oligonucleotides used in this study are listed in Table 6 and Table 1, respectively.

Construction of TAP-tagged strains. The yeast strains harboring the N-terminally TAP-tagged versions of WT Ypt1p and mutant Ypt1-3p proteins were generated by amplifying the TAP tag sequence using the plasmid pBS1761 (carrying TAP sequence) as the template. A pair of overhang primers were used in which the forward primer harbors the sequence corresponding to the 60 nucleotides upstream of the ATG codon (with the start codon) and the reverse primer carries the reverse complement of 60 nucleotides downstream of the Start codon of the *YPT1* gene.[48] The PCR product consisting of the TAP

TABLE 5 List of yeast strains used in this study

Strain	Genotype	Reference
yBD117	*Mata leu2-3,112 ura3-52 his3-Δ200 trp1-Δ901 lys2-801*	47
yBD118	*Mata leu2-3,112 ura3-52 his3-Δ200 trp1-Δ901 lys2-801 hac1::TRP1*	47
yBD129	*Mata leu2-3,112 ura3-52 his3- Δ200 trp1-Δ901 lys2-801 rrp6::URA3*	31
yBD131	*Mata leu2-3,112 ura3-52 his3- Δ200 trp1-Δ901 lys2-801 cbc1:: hisG*	31
yBD148	*MATa leu2-3,112 ura3-52 trp1-1 his3-11,15 nrd1Δ::HIS3; lys2Δ2; ade2-1; met2Δ1, can1-100 [pRS316NRD1 (NRD1, URA3, CEN)]*	35
yBD157	*MATα ura3Δ0 his3Δ1 leu2Δ0; met15Δ0 LYS2 nrd1Δ::KAN RRP6-TAP::HIS3 [pJC580 (NRD1-HA, LEU2, CEN)]*	35
yBD158	*MATα ura3Δ0 his3Δ1 leu2Δ0; met15Δ0; LYS2; nrd1Δ::KAN; RRP6-TAP::HIS3 [pJC720 (nrd1-102-HA, LEU2, CEN)]*	35
yBD177	*MATa ura3-52 leu2-3,112 trp1-1 his3-11,15 nrd1::HIS3 lys2Δ2 ade2-1 met2Δ1 can1-100[pRS 424 nrd1-1(nrd1-1, TRP1, 2 μ ori)]*	35
yBD276	*Mata ura3-52 leu2-3,112 his3-Δ200 trp1-Δ901 lys2-801 HIS3-GAL::protA-CBC1 (pGAL-CBC1)*	31
yBD433	*MATa ura3-52 leu2-3,112*	32
yBD434	*MATa ura3-52 leu2-3,112ypt1-3*	32
yBD457	*MATa ura3-52 leu2-3,112 YPT-TAP::URA3*	This study
yBD549	*Mata leu2-3,112 ura3-52 his3-Δ200 trp1-Δ901 lys2-801 hac1::TRP1 [pRS316 HAC1(HAC1,URA3, CEN)]*	This study
yBD550	*Mata leu2-3,112 ura3-52 his3-Δ200 trp1-Δ901 lys2-801hac1::TRP1 [pRS316 HAC1-ΔR1(HAC1-ΔR1,URA3,CEN)]*	This study
yBD551	*Mata leu2-3,112 ura3-52 his3-Δ200 trp1-Δ901 lys2-801 hac1::TRP1 [pRS316 HAC1-ΔR2(HAC1-ΔR2,URA3,CEN)]*	This study
yBD552	*Mata leu2-3,112 ura3-52 his3-Δ200 trp1-Δ901 lys2-801 hac1::TRP1 [pRS316 HAC1 ΔBE(HAC1-ΔBE,URA3,CEN)]*	This study
yBD553	*Mata leu2-3,112 ura3-52 his3-Δ200 trp1-Δ901 lys2-801 hac1::TRP1 [pRS316HAC1 Δ3′UTR(HAC1-Δ3′UTR,URA3,CEN)]*	This study
yBD565	*MATa ura3-52 TAP-ypt1-3::URA3*	This study
yBD572	*MATa ura3-52 leu2-3,112 trp1-1 his3-11,15 nrd1::HIS3 lys2Δ2 ade2-1 met2Δ1 can1-100 [pRS316 NRD1 (NRD1, URA3, CEN), pRS 315 TAP-YPT1(TAP-YPT1,LEU2,CEN)]*	This study
yBD573	*MATa ura3-52 leu2-3,112 trp1-1 his3-11,15 nrd1::HIS3 lys2Δ2 ade2-1 met2Δ1 can1-100, [pRS 424 nrd1-1(nrd1-1, TRP1, 2 μ ori), pRS 315 TAP-YPT1 (TAP-YPT1,LEU2,CEN)]*	This study
yBD579	*MATa ura3-52 ypt1-3 hac1::hisG[pRS316 HAC1-ΔR1(HAC1-ΔR1,URA3,CEN)]*	This study
yBD580	*MATa ura3-52 ypt1-3 hac1::hisG[pRS316 HAC1-ΔR2(HAC1-ΔR2,URA3,CEN)]*	This study
yBD581	*MATa ura3-52 ypt1-3 hac1::hisG[pRS316HAC1 Δ3′UTR(HAC1-Δ3′UTR,URA3,CEN)]*	This study
yBD582	*MATa ura3-52 ypt1-3 hac1::hisG[pRS316HAC1 Δ3′UTR(HAC1-ΔBE,URA3,CEN)]*	This study
yBD583	*Mata leu2-3,112 ura3-52 his3-Δ200 trp1-Δ901 lys2-801 hac1::TRP1 cbc1::hisG[pRS316 HAC1-ΔR1(HAC1-ΔR1,URA3,CEN)]*	This study
yBD584	*Mata leu2-3,112 ura3-52 his3-Δ200 trp1-Δ901 lys2-801 hac1::TRP1 cbc1::hisG[pRS316 HAC1-ΔR2(HAC1-ΔR2,URA3,CEN)]*	This study
yBD585	*Mata leu2-3,112 ura3-52 his3-Δ200 trp1-Δ901 lys2-801 hac1::TRP1 cbc1::hisG[pRS316 HAC1 ΔBE(HAC1-ΔBE,URA3,CEN)]*	This study
yBD588	*Mata leu2-3,112 ura3-52 his3-Δ200 trp1-Δ901 lys2-801 hac1::TRP1 [pRS 315 TAP-YPT1 (TAP-YPT1,LEU2,CEN), pRS316 HAC1(HAC1,URA3, CEN)]*	This study
yBD589	*Mata leu2-3,112 ura3-52 his3-Δ200 trp1-Δ901 lys2-801 hac1::TRP1[pRS 315 TAP-YPT1 (TAP-YPT1,LEU2,CEN), pRS316 HAC1-ΔR1(HAC1-ΔR1,URA3,CEN)]*	This study
yBD590	*Mata leu2-3,112 ura3-52 his3-Δ200 trp1-Δ901 lys2-801 hac1::TRP1[pRS 315 TAP-YPT1 (TAP-YPT1,LEU2,CEN), pRS316 HAC1-ΔR2(HAC1-ΔR2,URA3,CEN)]*	This study
yBD591	*Mata leu2-3,112 ura3-52 his3-△ 200 trp1-Δ901 lys2-801hac1::TRP1[pRS 315 TAP-YPT1 (TAP-YPT1,LEU2,CEN), pRS316 HAC1-ΔBE(HAC1-ΔBE,URA3,CEN)]*	This study
yBD592	*Mata leu2-3,112 ura3-52 his3-△ 200 trp1-Δ901 lys2-801 hac1::TRP [pRS 315 TAP-YPT1 (TAP-YPT1,LEU2,CEN), pRS316 HAC1-Δ3′UTR(HAC1-Δ3′UTR,URA3,CEN)]*	This study
yBD629	*Mata leu2-3,112 ura3-52 his3-Δ200 trp1-Δ901 lys2-801 hac1::TRP1 [pRS316 HAC1-R2-BE-R2 (HAC1-R2-BE-R2,URA3,CEN)]*	This study
yBD630	*Mata leu2-3,112 ura3-52 his3-Δ200 trp1-Δ901 lys2-801 hac1::TRP1 [pRS316 HAC1-R2-BE-R1 (HAC1-R2-BE-R1,URA3,CEN)]*	This study

TABLE 6 List of plasmids used in this study

Plasmid	Description	Reference
pBD42	*CBC1* disruptor, *pUC18 cbc1::URA*	17
pBD217	*ND-GFP2* in low-copy *LEU2 (Nucleolin domain)*	37
pBD218	*Ire1-RFP* in high-copy *LEU2* vector	37
pBD219	$HAC1^{NRE}$ in *pRS 316 URA3* vector	37
pBD93	*HAC1* disrupter; *pRS 316 hac1::URA*	This study
pBD95	*HAC1* inserted in the *Bam*HI site of *pRS 316*	This study
pBD220	*HAC1*-ΔBE *pRS 316 CEN*	38
pBD333	154 bp of 3′-UTR of *HAC1* was deleted from *pRS 316 HAC1* by reverse PCR using primer pair OBD 842 & OBD843	This study
pBD334	142 bp of 3′-UTR of *HAC1* was deleted from *pRS 316 HAC1* by reverse PCR using primer pair OBD 844 & OBD845.	This study
pBD335	379 bp of *HAC1* 3′UTR (1–379) was deleted from *pRS 316 HAC1* by reverse PCR using primer pair OBD 842 & OBD 845.	This study
pBD342	TAP-Ypt1 tagged gene cloned in Sma1 site of *pRS 315 LEU2 CEN*	This study

sequence flanked by the 60 nucleotides upstream of the ATG codon and the 60 nucleotides downstream of the start codon of the of *YPT1* gene was integrated into the genomic locus of *YPT1* or *ypt1-3* alleles following the transformation into appropriate yeast strains using two-step gene replacement procedure.

Construction of various deleted versions *HAC1* allele. For the construction of various deleted versions of 3′-UTR of the *HAC1* allele reverse PCR technology was employed. In this technique, cloned version of the *HAC1* gene in a *CEN* plasmid along with its 3′-UTR sequence in plasmid used as template was subjected to PCR reaction with Q5®High-Fidelity DNA Polymerase (New England Biolabs Inc., MA, USA) with a set of forward and reverse primers flanking the region to be deleted. However, in contrast to traditional PCR, in this PCR, the sense primer was placed downstream and the antisense primer was positioned upstream of the region to be deleted. PCR amplification of the template using these primer sets resulted in the entire *HAC1* gene in the same plasmid backbone without the deleted region. The PCR products thus obtained from various PCR reactions were purified from the gel, ligated using T4 DNA Ligase (New England Biolabs Inc., MA, USA), and transformed in *hac1*-Δ yeast strain along with a full-length *HAC1* control.

Cell viability assay. Cell viability assay was performed as described previously.[49] Briefly, each strain was grown overnight, and the culture was then subsequently diluted to 1×10^7 cells/mL. This stock was further diluted 10-fold serially to achieve 1×10^4, 1×10^3, and 1×10^2 cells/mL respectively. 3 μL of each stock was then spotted onto the surface of the YPD plate (yeast extract 1%, peptone 2%, dextrose 2%, agar 2%) without and with 1 μg/mL tunicamycin (Sigma-Aldrich Inc., MI, USA). Plates were then incubated for 48–72 h at 30 °C before capturing their photographs. For liquid growth assay, specific strains of *S. cerevisiae* were grown in triplicate until the OD_{600} reaches 0.6 and each culture was divided into two parts. In one-half of the culture, either DTT or tunicamycin was added to a final concentration of 5 mM (+DTT) or 1 μg/mL respectively, whereas an equal volume of DMSO (mock-treated, -Tm/-DTT) was added to the other half of the culture. Cultures were continued to grow and 100 μL of aliquots were withdrawn at indicated times after DTT/tunicamycin addition and were spread onto a solid YPD plate. Plates were then incubated for 48–72 h at 30 °C and the total number of colonies for a specific strain was counted and plotted as a histogram. The number of colonies obtained on the plates of 0 h (at the time of addition of tunicamycin/DTT) in each case was set to one.

RNA analyses and determination of steady-state and decay rate of mRNAs. Total RNA was isolated as described earlier[18] by harvesting appropriate yeast strains followed by extracting the cell suspension in the presence of phenol-chloroform-IAA (25:24:1) and glass bead. Following the extraction, the RNA was recovered by precipitation with RNAase-free ethanol.

For the preparation of cDNA, total RNA samples were first treated with 1 μg RNAase free DNase I (Fermentas Inc., MA, USA) at 37 °C for 30 min followed by first strand cDNA synthesis using Superscript Reverse Transcriptase (Thermo Fisher Scientific Inc., MA, USA) using Random Primer (Bioline Inc.) by incubating the reaction mixture at 50 °C for 30 min. Real-time qPCR analyses with 2 to 3 ng of cDNA samples were used to determine the steady-state levels of pre-*HAC1*, *SCR1*, etc. were performed as described previously.[31]

Stability of a specific mRNA were determined by the inhibition of global transcription with transcription inhibitor 1, 10 phenanthroline (Sigma-Aldrich Inc., MI, USA) at 30 °C, as described previously.[18] Briefly, the specific strain was grown at 30 °C till the mid-logarithmic phase, and 1,10 phenanthroline was then added to the growing culture at 20 μg/mL final concentration followed by withdrawal of a 25 mL of an aliquot of culture at various times after transcription shut-off. Total RNA was isolated from each time-point aliquot followed by the preparation of cDNA samples as described above. Levels of pre-*HAC1* and other specific mRNAs were quantified from respective cDNA samples by RT-qPCR analysis using the primer sets corresponding either to pre-*HAC1* intronic sequences or to other mRNAs. The intronic signals of pre-*HAC1* were normalized to *SCR1* RNA signals obtained for each time point and the normalized signals (mean values ± SD) were presented as the fraction of remaining pre-*HAC1* RNA (with respect to normalized signals at 0 min) as a function of time after shutting-off the transcription of RNA polymerase II by the addition of 1, 10-phenanthroline. The decay rates and half-lives of specific mRNAs were estimated using the normalized RNA signals with the regression analysis program (GraphPad Prism

TABLE 7 List of antibodies used in this study and their sources

Sl. no.	Name of the primary antibody	Source	Primary antibody dilution	Secondary antibody	Secondary antibody dilution
1	Anti-TAP	Commercially Procured, Thermo Scientific	1:1000	Anti-Rabbit	1:3000
2	Anti-Rrp6	Dr Scott Butler, University of Rochester, NY, USA	1:1000	Anti-Rabbit	1:3000
3	Anti-Cbc1	Dr Scott Butler, University of Rochester, NY, USA	1:1000	Anti-Rabbit	1:3000
4	Anti-Rrp4	Dr Scott Butler, University of Rochester, NY, USA	1:1500	Anti-Rabbit	1:3000
5	Anti-Tif4631	Dr Julie Baron-Benhamou, Rockefeller University, New York, USA	1:2000	Anti-Rabbit	1:3000
6	Anti-Nrd1	Dr. Stephen Buratowski, Harvard Medical School, Boston, MA, USA	1:1000	Anti-Rabbit	1:3000
7	Anti-Nab3	Dr Maurice S. Swanson, University of Florida, Gainesville, FL, USA	1:1000	Anti-Mouse	1:3000

version 8.0.1) using a single exponential decay formula (assuming mRNA decay follows a first order kinetics), $y = a(1 - b)^x$ was used, wherein y = final amount, a = initial amount, b = decay constant and x = time that has passed.

Immunoblot analysis. Total protein was isolated from specific yeast strains grown overnight at 30 °C in YPD broth. Following the harvesting by centrifugation at 5000 rpm for 7 min the cell pellets were quickly frozen in liquid nitrogen and stored at −70 °C. Frozen pellets were thawed on ice and resuspended in 1 mL of Buffer A (50 mM Tris-HCl pH 7.5, 150 mM NaCl, 5 mM EDTA, 1 mM DTT, 1 mM PMSF) supplemented with protease inhibitor (Invitrogen Inc., Carlsbad, CA, USA) and the cells were lysed by vortexing 10–15 times with glass beads followed by clarification of the particulate fraction by centrifugation. Supernatants were collected by centrifugation at 10,000 rpm for 20 min and saved as the total soluble protein fraction for further analysis. Protein concentration was determined by Bradford reagent assay kit (Bio-Rad Inc., Valencia, CA, USA). 30–50 μg of total protein was used, which was resolved either in an 8% or a 10% SDS-polyacrylamide gel and then immunoblot analysis using primary antibodies for specific proteins for 1 h at room temperature in the following dilutions: rabbit polyclonal anti-TAP (cat.#CAB1001) (1:1000), rabbit polyclonal anti-Cbc1 (1:1000), rabbit polyclonal anti-Rrp6 (1:1000), rabbit polyclonal anti-Tif4631 (1:2000), rabbit polyclonal anti-Rrp4 (1:1000) (Table 7). Immunoreactive bands were developed and detected by chemiluminescence (ECL imager kit, Abcam) and the images were captured either by X-ray film or myECL Chemidoc Imager (Thermo Scientific, USA).

RNA-chromatin immunoprecipitation (RNA-ChIP). RNA-chromatin preparation (RNA-ChIP) was performed as described earlier.[35] The *YPT1* and *ypt1-3* strains or *NRD1* and *nrd1-1* strains in the different backgrounds were used for this study 150 mL of cells grown until $OD_{600} \approx 0.5$ ($\approx 10^7$ cells/mL) and were fixed with 1% formaldehyde for 20 min. After glycine addition to stop the reaction, the cells were washed and lysed with glass beads to isolate chromatin. The cross-linked chromatin was sheared by sonication to reduce the average fragment size to ≈ 500 bp. Immunoprecipitation of chromatin was carried out using a ChIP assay kit (EZ-ChIP™; Catalog No. 17-295, Millipore Sigma, MA, USA). Immunoprecipitation of 120 μg Chromatin fractions (≈100 μL) from each strain was performed with protein G agarose and specific antibody overnight at 4 °C. After washing beads and chromatin elution, the eluted supernatants and the input controls were incubated with proteinase K for 1h at 37 °C followed by 5 h at 65 °C to reverse crosslink DNA complexes. DNA was extracted using the DNA-clean-up column provided with the kit. The immunoprecipitated DNAs (output) were quantitated by real-time PCR using specific primers located along a specific gene coding sequence and normalized to a half dilution of input DNA. Amplifications were done in triplicate for each sample, and averages and standard deviations were calculated based on three independent experiments.

Analysis of binding profile of mRNA by RNA immunoprecipitation. Yeast strains containing N-terminally TAP-tagged *YPT1* cells or other cells were grown until the OD_{600} of the culture reached 0.6 to 0.8. Before the lysis of the cells, intact yeast cells were cross-linked by UV-irradiation in a petri dish on ice. Cells were washed once with Buffer A (50 mM Tris-HCl pH 7.4, 140 mM NaCl, 1.8 mM $MgCl_2$, 0.1% NP-40), resuspended in Buffer B (Buffer A supplemented with 0.5 mM DTT, 40 U/mL RNase inhibitor, 1 mM PMSF, 0.2 mg/mL heparin, protease inhibitor) and lysed by vortexing using glass beads. Lysates were cleared by centrifugation for 10 min at 8,000 rpm at 4 °C. The lysate was quantified and precleared for 30 min at 4 °C. Protein A Sepharose beads (Santa Cruz Biotechnology, TX, USA) were coated overnight at 4 °C using TAP antibody (Cat#CAB1001) (Thermo Fisher Scientific, MA, USA) in Buffer B. One mg precleared cell lysate was incubated with antibody-coated beads for 4 h at 4 °C on a rotator. Beads were washed twice in Buffer B for 5 min/4 °C/rotator each, and once in Buffer C (50 mM Tris pH-7.4, 140 mM NaCl, 1.8 mM $MgCl_2$, 0.01% NP-40, 10% glycerol, 1 mM PMSF, 0.5 mM DTT, 40 U/mL RNase inhibitor, protease inhibitor) for 5 min at 4 °C rotator each. After washing, beads were resuspended in 200 μL Buffer C supplemented with 1% final SDS and heated at 70 °C for 45 min with constant mixing to de-crosslink samples and elute antibody-bound protein-RNA complexes from the beads. Cells for "Mock IP" from an isogenic parental untagged strain were grown, cross-linked, lysed, and incubated with anti-TAP antibody

and protein A plus Sepharose beads following the same procedure. Finally, RNA was isolated from the eluates by phenol-chloroform-isoamyl alcohol (25:24:1) extraction at pH 4.5, and cDNA was prepared using first strand cDNA synthesis kit (Takara Bio Inc., Shiga, Japan) as described above. The immunoprecipitated RNAs (output) were quantitated by real-time PCR using specific primers located along a specific gene coding sequence and normalized to a half dilution of input DNA. Amplifications were done in triplicate for each sample, and averages and standard deviations were calculated based on three independent experiments.

Coimmunoprecipitation. Cells were grown in 50 mL YPD until OD_{600} 2.7–3.0 is reached. The cell lysate was prepared as described previously in 1 mL of Buffer A. Protein A^{PLUS} Agarose Beads (Santa Cruz Biotechnology, TX, USA) ~20 μL bed volume per reaction were equilibrated twice with 10 volumes of Buffer A. The beads for each washing were resuspended in Buffer A and kept on a rotator wheel for 5 min at 4 °C. The beads were centrifuged each time to remove residual Buffer A. The extract was then precleared by adding the equilibrated beads and incubation on a rotator wheel at 4 °C for 30 min followed by centrifugation to get rid of the beads. To the precleared protein extract, a specific antibody was added and incubated for 4 h on a rotator wheel at 4 °C. To this extract, a 50 μL bed volume of pre-equilibrated Protein A^{PLUS} Agarose Beads was added and incubated at 4 °C on the rotator wheel overnight. The beads were washed three times with 10 volumes of Buffer A by rotating on the rotator wheel at 4 °C for 10 min each. Finally, elution was performed by boiling the beads in 40 μL of SDS loading dye for 5 min. Samples were then analyzed on 12% SDS-PAGE gel followed by Western blot analysis.

StreptoTag affinity chromatography. The StreptoTag (streptomycin-binding aptamer) affinity purification was essentially carried out as described before.[38,50] Briefly, ethanol/NaOH treated epoxy-activated Sepharose 6B was coupled with dihydrostreptomycin followed by immobilizing 50–500 pmol hybrid RNA by incubating at 56 °C for 5 min followed by 37 °C for 10 min in 100 μL column buffer (50 mM Tris HCl, pH 7.5, 5 mM $MgCl_2$, 250 mM NaCl). 1 mg of total cellular protein extract was incubated with the refolded hybrid mRNA for 2.5 h at 4 °C. The mixture was then loaded onto the column and incubated within the column for 45 min for binding. The proteins that bind to this hybrid RNA were then eluded with 1 mL column buffer containing 10 μM streptomycin. The eluted proteins were then precipitated with one volume of 100% trichloro acetic acid (TCA) followed by incubation for 10 min at 4 °C and centrifugation at 10,000 rpm for 5 min. The protein pellet was then washed with 200 μL cold acetone followed by centrifugation at 15,000 rpm for 5 min. The pellet was then dried in a 95 °C heat block for 5 min and was finally dissolved in a suitable buffer solution and was run on SDS-PAGE and subjected to Western blot analysis.

In Vitro RNA-protein binding analysis by electrophoretic mobility shift assay (EMSA). For the EMSA experiment, two different segments corresponding to R1 and R2 regions of *HAC1* mRNA along with T7 promoter sequence were separately amplified by regular PCR and thereafter transcribed *in vitro* with T7 RNA polymerase using T7 Ribomax™ Express Kit following the instructions of the manufacturer (Catalog No. P1320, Promega Corporation, Madison, USA) to produce R1 and R2 RNA segments. Sixty-five micrograms of each of these *in vitro* transcribed R1 and R2 RNA segments were incubated with the reaction mixture consisting of 1 mM spermidine, 5X gel shift buffer (70 mM HEPES pH 7.9, 450 mM KCl, 11 mM $MgCl_2$, 28% glycerol), 20 U RNase inhibitor, and different concentrations (0, 5, 10, and 20 μg) of protein extracts prepared from yeast strains expressing either functional Ypt1p or mutant Ypt1–3p were mixed and incubated for 30 min at 30 °C. The reaction mixture was transferred to ice for 5 min followed by mixing the binding reaction with 6X loading buffer (30% glycerol, 0.3% bromophenol blue, 0.3% xylene cyanol) and electrophoresis on a 15% nondenaturing gel for 2 to 3 h at 200 V at 4 °C followed by staining the gel with ethidium bromide and visualizing it under a UV-Gel documentation imager.

Localization analysis of *HAC1^{NRE}-GFP* mRNA and Ire1p-RFP proteins using confocal microscopy and image processing. The colocalization imaging of *HAC1* mRNA with Ire1 proteins in the live cell was done by using three plasmids[37] as described earlier.[31] The reporter plasmid (pBD219, Table 6) carries an engineered version of *HAC1* mRNA in which a 22-nucleotide RNA module, identical to the nucleolin recognition element (NRE) was inserted at the 3′-UTR (*HAC1^{NRE}*). The second plasmid (pBD217, Table 6) expressed a chimeric protein consisting of an NRE-binding nucleolin domain (ND) which is fused to the monomeric form of the green fluorescent protein 2 (GFP2). In the third plasmid (pBD218, Table 6), Ire1p is conjugated with a red fluorescent protein (RFP). All these plasmids were transformed into an appropriate yeast strain and were grown until the OD_{600} reaches 0.6. 1 μg/mL of tunicamycin was then added to the medium and incubated for another 30 min at 30 °C. An aliquot of the cell was used for *in vivo* imaging studies. Images were captured using Confocal Laser Scanning Microscope (Leica Stellaris 5). The GFP and RFP were excited at 458 nm and 514 nm respectively, and emissions were recorded at 466–526 nm and 530–650 nm respectively. Image processing and analysis of colocalization Index were estimated using Leica Microsystem Software (LAS X Version 4.5.0.25531). For calculating the colocalization indices of the *HAC1$^{NRE\text{-}GFP}$* mRNA and Ire1p-RFP in WT and *ypt1-3* strains, pixel intensities of the mRNA (green), Ire1p (red) and the merged signal of mRNA/Ire1p together (yellow) from specific Z-section of every cell were used by the software to calculate Pearson's correlation coefficient. Eight independent biological replicates of each of WT and *ypt1-3* strains were performed and red, green and yellow signals from 5 to 8 cells from each replicate (a total of 25–40 cells in total for each of WT and *ypt1-3* strains) were used by the software to calculate colocalization index. The mean values of colocalization indices from each replicate are presented in Table 2 and the final histogram presented in Fig. 5B are derived from these mean values.

Flow cytometry-based FRET. Flow cytometry-based fluorescence resonance energy transfer (FRET) measurement was performed using the protocol described earlier.[51] The amount of signal quenched in the presence of an acceptor from a donor is considered the indicator of quantitative FRET, where the donor-acceptor pair have a significant overlap of excitation spectra of acceptor and emission spectra of

donor. In our case, *GFP2* as part of the bound *HAC1*^{NRE}-GFP-nucleolin module and RFP as part of Ire1-RFP fluorophores serve as the donors and acceptors respectively. The appropriate strain harboring all three plasmids i.e. *HAC1*^{NRE}, GFP2-nucleolin, and Ire1-RFP, or only GFP2-nucleolin was grown until the OD_{600} of the culture reaches 0.6 in the selective medium along with the unlabeled cell. Tunicamycin was added to each culture to the final concentration of 1 μg/mL and aliquots of cells were harvested at 30 min after the addition of tunicamycin. Fluorescence intensities of each sample were determined by a single laser GFP filter (FL1) of BD Verse Flow Cytometer. Mean fluorescence intensity is calculated by BD Accuri™ C6 software by taking 10,000 cells/sample. Average FRET efficiency (E) of the measured population according to the following equation:

$$\mathbf{E} = 1 - \frac{(\mathbf{I_{DA}} - \mathbf{I_0})}{(\mathbf{I_D} - \mathbf{I_0})}$$

Where I_{DA} is the fluorescence intensity of the donor-acceptor sample, I_D is the fluorescence intensity of the donor-only sample, and I_0 is the fluorescence intensity of the unlabeled sample. To calculate the FRET value, five independent biological replicates of each of the WT and *ypt1-3* strains were carried out and three technical replicates under each biological replicates were done. The average FRET values of each of the three technical replicates from one biological replicate are presented in Table 3. The mean FRET values of five biological replicates were finally used to calculate the Mean FRET of WT and *ypt1-3* strains, which is presented as the histogram in Fig. 5C.

Localization of Ypt1p by indirect immunofluorescence. Cells were grown in 10 mL culture tubes up to the mid-log phase (OD_{600} = 0.6) followed by addition of DMSO (unstressed) or tunicamycin (stressed) to final concentration of 1 μg/mL. Cells then continued to grow for another 30 min in the presence and in the absence of tunicamycin and 4% paraformaldehyde was added to each culture for fixation, which was continued for 30 min followed by harvesting of the cells. Cells are then washed twice in 0.1 M KPO_4 buffer and once in 0.1 M KPO_4/1.2 M sorbitol and finally resuspended in 1 mL 0.1 M KPO_4/1.2 M Sorbitol. The cells were then spheroplasted for permeabilization by mixing 0.5 mL cells with 5 μL of 10 mg/mL Lyticase (Sigma-Aldrich Inc., MI, USA) and 10 μL β-mercaptoethanol (Sigma-Aldrich Inc., MI, USA) followed by incubation at 30 °C for 10–20 min as per cell density. The reaction was supplemented with 10 μL of β-mercaptoethanol for optimal reaction. After an adequate amount of spheroplasting, cells were centrifuged at 5000 rpm for 1 min and washed gently with 0.1 M KPO_4/1.2 M sorbitol twice and finally resuspended in 200 μL of KPO_4/1.2 M medium. Cells are now ready to adhere onto polylysine coated coverslips (regular glass slips are appropriately polylysine coated according to the Manufacturer's protocol). About 100 μL of spheroplasted cells are added onto the polylysine coated coverslips and allowed to sit for 15–20 min. After aspirating out the supernatant cells are blocked with 400 μL of 10% PBS-BSA for 30 min followed by the addition of primary antibody (anti-TAP antibody at 1:200). Cells are incubated overnight at 4 °C in a humid chamber. The cells were then washed five times with PBS-BSA before incubation with a secondary antibody (goat anti-rabbit secondary antibody, FITC, Cat #F-2765 at 1:1000) at room temperature in the dark for 1 h. The cells were washed further four times with PBS-BSA followed by incubating the cells with 1.5 μg/mL Hoechst to stain the nucleus. The cells were then washed extensively with PBS-BSA and finally mounted onto a clean glass slide using 10 mg/mL p-phenylenediamine (Sigma) in 90% glycerol. The cells were observed in Confocal Laser Scanning Microscope (Leica Stellaris 5) and the localization of *YPT1* was analyzed from the FITC. Briefly, for WT and *ypt1-3* strains (both in the absence and in the presence of tunicamycin) six independent biological replicates were carried out and 5–8 cells from different fields from each replicate were analyzed (a total of 25–40 cells were analyzed for each strain in total under a specific condition). For every cell, the specific green signal (TAP-Ypt1p/FITC), blue (nuclear distribution/Hoechst), and image of the merged signal of Ypt1p and nuclear distribution from every Z-section were processed for the final computation of the colocalization data by Leica Microsystems Software (LAS X Version 4.5.0.25531) as mentioned above. The mean colocalization index values of each of these biological replicates are presented in Table 4 and the histogram presented in Fig. 8C and D are derived from these values.

Statistical analyses. All the quantitative experiments reported in this paper (mRNA steady-state levels, decay rates, chromatin immunoprecipitation, RNA immunoprecipitation experiments, quantitative growth experiments in liquid media) were done from at least three independent biological replicates (n = 3). However, for calculating the colocalization index, the sample sizes are either eight (n = 8) or six (n = 6) and for determination of FRET, the sample size was five (n = 5). All the statistical parameters such as mean, standard deviations, *P* values, and standard error of the mean were estimated using GraphPad Prism version 8.0.1. *P* values were determined using paired Student's two-tailed *t* test.

ACKNOWLEDGMENTS

We acknowledge Dr Randy W. Schekman (University of California, Berkeley) for sharing the *ypt1-3* mutant yeast strain and Dr Stephen Buratowski (Harvard Medical School, Boston, MA, USA) for sharing the *nrd1-1* mutant strain, and anti-Nrd1 antibody. We also acknowledge Dr Scott Butler for providing us with the Anti-Rrp6p, Anti-Rrp4p, Anti-Cbc1p, and Anti-Tif4631 antibodies (the University of Rochester, Rochester, NY, USA) and Dr. Maurice Swanson (the University of Florida, Gainesville, Fl, USA) for sharing Anti-Nab3 antibody. We thank Dr Satarupa Das and the members of the Das Laboratory for critically reading this manuscript. We also thank the anonymous reviewers for their critical comments and constructive suggestions.

AUTHOR CONTRIBUTIONS

SP and AC conducted all the experiments. SP and BD conceived and designed all the experiments, BD directed the research program, organized and wrote the manuscript.

FUNDING

This investigation was supported by research grants from SERB, the Government of India (Award No. CRG/2021/005449 to BD), and Jadavpur University (RUSA 2.0 Research Grant) to BD. SP was supported by the DST-PURSE Phase II program from DST, Government of India.

ORCID

Sunirmal Paira http://orcid.org/0000-0002-6910-4129
Anish Chakraborty http://orcid.org/0009-0002-1706-875X
Biswadip Das http://orcid.org/0000-0002-2839-2048

DATA AVAILABILITY STATEMENT

The authors state that the data supporting the findings of this study are available at: Paira Sunirmal; Chakraborty Anish, and Das Biswadip. (2023) "Paira S. et al. (2023) The sequential recruitments of Rab-GTPase Ypt1p and the NNS complex onto pre-*HAC1* mRNA promote its nuclear degradation in baker's yeast", Mendeley Data, https://data.mendely.com/datasets/ry4v78z2tx/1.

REFERENCES

1. Fasken MB, Corbett AH. Links between mRNA splicing, mRNA quality control, and intellectual disability. RNA Dis. 2016;3:e1448.
2. Houseley J, LaCava J, Tollervey D. RNA-quality control by the exosome. Nat Rev Mol Cell Biol. 2006;7:529–539. doi:10.1038/nrm1964.
3. Parker R. RNA degradation in Saccharomyces cerevisae. Genetics. 2012; 191:671–702. doi:10.1534/genetics.111.137265.
4. Das S, Das B. MRNA quality control pathways in *Saccharomyces cerevisiae*. J Biosci. 2013;38:615–640. doi:10.1007/s12038-013-9337-4.
5. Singh P, Saha U, Paira S, Das B. Nuclear mRNA surveillance mechanisms: function and links to human disease. J Mol Biol. 2018;430:1993–2013. doi: 10.1016/j.jmb.2018.05.009.
6. Butler JS. The yin and yang of the exosome. Trends Cell Biol. 2002;12:90–96. doi:10.1016/s0962-8924(01)02225-5.
7. Liu Q, Greimann JC, Lima CD. Reconstitution, activities, and structure of the eukaryotic RNA exosome. Cell. 2006;127:1223–1237. doi:10.1016/j.cell.2006.10.037.
8. Wasmuth EV, Januszyk K, Lima CD. Structure of an Rrp6-RNA exosome complex bound to poly(A) RNA. Nature. 2014;511:435–439. doi:10.1038/nature13406.
9. Kilchert C, Wittmann S, Vasiljeva L. The regulation and functions of the nuclear RNA exosome complex. Nat Rev Mol Cell Biol. 2016;17:227–239. doi:10.1038/nrm.2015.15.
10. Zinder JC, Wasmuth EV, Lima CD. Nuclear RNA exosome at 3.1 A reveals substrate specificities, RNA paths, and allosteric inhibition of Rrp44/Dis3. Mol Cell. 2016;64:734–745. doi:10.1016/j.molcel.2016.09.038.
11. Wasmuth EV, Zinder JC, Zattas D, Das M, Lima CD. Structure and reconstitution of yeast Mpp6-nuclear exosome complexes reveals that Mpp6 stimulates RNA decay and recruits the Mtr4 helicase. Elife. 2017;6:e29062. doi:10.7554/eLife.29062.
12. Kadaba S, Krueger A, Trice T, Krecic AM, Hinnebusch AG, Anderson J. Nuclear surveillance and degradation of hypomodified initiator tRNA Met in *S. cerevisiae*. Genes Dev. 2004;18:1227–1240. doi:10.1101/gad.1183804.
13. Wlotzka W, Kudla G, Granneman S, Tollervey D. The nuclear RNA polymerase II surveillance system targets polymerase III transcripts. Embo J. 2011; 30:1790–1803. doi:10.1038/emboj.2011.97.
14. Schmidt K, Butler JS. Nuclear RNA surveillance: role of TRAMP in controlling exosome specificity. Wiley Interdiscip Rev RNA. 2013;4:217–231. doi: 10.1002/wrna.1155.
15. Hardwick SW, Luisi BF. Rarely at rest: RNA helicases and their busy contributions to RNA degradation, regulation and quality control. RNA Biol. 2013;10:56–70. doi:10.4161/rna.22270.
16. Halbach F, Reichelt P, Rode M, Conti E. The yeast ski complex: crystal structure and RNA channeling to the exosome complex. Cell. 2013;154: 814–826. doi:10.1016/j.cell.2013.07.017.
17. Das B, Guo Z, Russo P, Chartrand P, Sherman F. The role of nuclear cap binding protein Cbc1p of yeast in mRNA termination and degradation. Mol Cell Biol. 2000;20:2827–2838. doi:10.1128/MCB.20.8.2827-2838.2000.
18. Das S, Saha U, Das B. Cbc2p, Upf3p and eIF4G are components of the DRN (degradation of mRNA in the nucleus) in *Saccharomyces cerevisiae*. FEMS Yeast Res. 2014;14:922–932. doi:10.1111/1567-1364.12180.
19. Maity A, Chaudhuri A, Das B. DRN and TRAMP degrade specific and overlapping aberrant mRNAs formed at various stages of mRNP biogenesis in *Saccharomyces cerevisiae*. FEMS Yeast Res. 2016;16:fow088. doi:10.1093/femsyr/fow088.
20. Arigo JT, Carroll KL, Ames JM, Corden JL. Regulation of yeast NRD1 expression by premature transcription termination. Mol Cell. 2006;21: 641–651. doi:10.1016/j.molcel.2006.02.005.
21. Conrad NK, Wilson SM, Steinmetz EJ, Patturajan M, Brow DA, Swanson MS, Corden JL. A yeast heterogeneous nuclear ribonucleoprotein complex associated with RNA polymerase II. Genetics. 2000;154:557–571. doi: 10.1093/genetics/154.2.557.
22. Steinmetz EJ, Conrad NK, Brow DA, Corden JL. RNA-binding protein Nrd1 directs poly(A)-independent 3′-end formation of RNA polymerase II transcripts. Nature. 2001;413:327–331. doi:10.1038/35095090.
23. Steinmetz EJ, Brow DA. Control of pre-mRNA accumulation by the essential yeast protein Nrd1 requires high-affinity transcript binding and a domain implicated in RNA polymerase II association. Proc Natl Acad Sci U S A. 1998;95:6699–6704. doi:10.1073/pnas.95.12.6699.
24. Singh P, Chaudhuri A, Banerjea M, Marathe N, Das B. Nrd1p identifies aberrant and natural exosomal target messages during the nuclear mRNA surveillance in *Saccharomyces cerevisiae*. Nucleic Acids Res. 2021; 49:11512–11536. doi:10.1093/NAR/GKAB930.
25. Kuai L, Das B, Sherman F. A nuclear degradation pathway controls the abundance of normal mRNAs in *Saccharomyces cerevisiae*. Proc Natl Acad Sci USA. 2005;102:13962–13967. doi:10.1073/pnas.0506518102.
26. Lee KPK, Dey M, Neculai D, Cao C, Dever TE, Sicheri F. Structure of the dual enzyme Ire1 reveals the basis for catalysis and regulation in nonconventional RNA splicing. Cell. 2008;132:89–100. doi:10.1016/j.cell.2007.10.057.
27. Sidrauski C, Walter P. The transmembrane kinase Ire1p is a site-specific endonuclease that initiates mRNA splicing in the unfolded protein response. Cell. 1997;90:1031–1039. doi:10.1016/s0092-8674(00)80369-4.

28. Kohno K, Normington K, Sambrook J, Gething MJ, Mori K. The promoter region of the yeast KAR2 (BiP) gene contains a regulatory domain that responds to the presence of unfolded proteins in the endoplasmic reticulum. Mol Cell Biol. 1993;13:877–890. doi:10.1128/MCB.13.2.877.
29. Aragón T, Van Anken E, Pincus D, Serafimova IM, Korennykh AV, Rubio CA, Walter P. Messenger RNA targeting to endoplasmic reticulum stress signalling sites. Nature. 2009;457:736–740. doi:10.1038/nature07641.
30. Rüegsegger U, Leber JH, Walter P. Block of HAC1 mRNA translation by long-range base pairing is released by cytoplasmic splicing upon induction of the unfolded protein response. Cell. 2001;107:103–114. doi:10.1016/S0092-8674(01)00505-0.
31. Sarkar D, Paira S, Das B. Nuclear mRNA degradation tunes the gain of the unfolded protein response in *Saccharomyces cerevisiae*. Nucleic Acids Res. 2018;46:1139–1156. doi:10.1093/nar/gkx1160.
32. Tsvetanova NG, Riordan DP, Brown PO. The yeast Rab GTPase Ypt1 modulates unfolded protein response dynamics by regulating the stability of HAC1 RNA. PLoS Genet. 2012;8:e1002862. doi:10.1371/journal.pgen.1002862.
33. Jedd G, Richardson C, Litt R, Segev N. The Ypt1 GTPase is essential for the first two steps of the yeast secretory pathway. J Cell Biol. 1995;131:583–590. doi:10.1083/JCB.131.3.583.
34. Steinmetz EJ, Brow DA. Repression of gene expression by an exogenous sequence element acting in concert with a heterogeneous nuclear ribonucleoprotein-like protein, Nrd1, and the putative helicase Sen1. Mol Cell Biol. 1996;16:6993–7003. doi:10.1128/mcb.16.12.6993.
35. Vasiljeva L, Buratowski S. Nrd1 interacts with the nuclear exosome for 3′ processing of RNA polymerase II transcripts. Mol Cell. 2006;21:239–248. doi:10.1016/j.molcel.2005.11.028.
36. Matabishi-Bibi L, Challal D, Barucco M, Libri D, Babour A. Termination of the unfolded protein response is guided by ER stress-induced HAC1 mRNA nuclear retention. Nat Commun. 2022;13:6331. doi:10.1038/s41467-022-34133-8.
37. Anshu A, Mannan MA, Chakraborty A, Chakrabarti S, Dey M. A novel role for protein kinase Kin2 in regulating HAC1 mRNA translocation, splicing, and translation. Mol Cell Biol. 2015;35:199–210. doi:10.1128/mcb.00981-14.
38. Windbichler N, Schroeder R. Isolation of specific RNA-binding proteins using the streptomycin-binding RNA aptamer. Nat Protoc. 2006;1:637–640. doi:10.1038/nprot.2006.95.
39. Wuestehube LJ, Duden R, Eun A, Hamamoto S, Korn P, Ram R, Schekman R. New mutants of *Saccharomyces cerevisiae* affected in the transport of proteins from the endoplasmic reticulum to the Golgi complex. Genetics. 1996;142:393–406. doi:10.1093/GENETICS/142.2.393.
40. Lynch-Day MA, Bhandari D, Menon S, Huang J, Cai H, Bartholomew CR, Brumell JH, Ferro-Novick S, Klionsky DJ. Trs85 directs a Ypt1 GEF, TRAPPIII, to the phagophore to promote autophagy. Proc Natl Acad Sci U S A. 2010;107:7811–7816. doi:10.1073/PNAS.1000063107.
41. Cole CN, Hammell CM. Nucleocytoplasmic transport: driving and directing transport. Curr Biol. 1998;8:R368–R372. doi:10.1016/s0960-9822(98)70239-8.
42. Grant PA, Schieltz D, Pray-Grant MG, Steger DJ, Reese JC, Yates JR, Workman JL. A subset of TAF II s are integral components of the SAGA complex required for nucleosome acetylation and transcriptional stimulation. Cell. 1998;94:45–53. doi:10.1016/S0092-8674(00)81220-9.
43. Goffin L, Vodala S, Fraser C, Ryan J, Timms M, Meusburger S, Catimel B, Nice EC, Silver PA, Xiao C-Y, et al. The unfolded protein response transducer Ire1p contains a nuclear localization sequence recognized by multiple β importins. Mol Biol Cell. 2006;17:5309–5323. doi:10.1091/MBC.E06-04-0292.
44. Pincus D, Chevalier MW, Aragon T, van Anken E, Vidal SE, El-Samad H, Walter P. BiP binding to the ER-stress sensor Ire1 tunes the homeostatic behavior of the unfolded protein response. PLoS Biol. 2010;8:e1000415. doi:10.1371/journal.pbio.1000415.
45. Rubio C, Pincus D, Korennykh A, Schuck S, El-Samad H, Walter P. Homeostatic adaptation to endoplasmic reticulum stress depends on Ire1 kinase activity. J Cell Biol. 2011;193:171–184. doi:10.1083/jcb.201007077.
46. Sherman F. Getting started with yeast. Methods Enzymol. 1991;194:3–21. doi:10.1016/0076-6879(91)94004-V.
47. Mori K, Kawahara T, Yoshida H, Yanagi H, Yura T. Signalling from endoplasmic reticulum to nucleus: transcription factor with a basic-leucine zipper motif is required for the unfolded protein-response pathway. Genes Cells. 1996;1:803–817. doi:10.1046/j.1365-2443.1996.d01-274.x.
48. Puig O, Caspary F, Rigaut G, Rutz B, Bouveret E, Bragado-Nilsson E, Wilm M, Séraphin B. The tandem affinity purification (TAP) method: a general procedure of protein complex purification. Methods. 2001;24:218–229. doi:10.1006/METH.2001.1183.
49. Back SH, Schröder M, Lee K, Zhang K, Kaufman RJ. ER stress signaling by regulated splicing: IRE1/HAC1/XBP1. Methods. 2005;35:395–416. doi:10.1016/j.ymeth.2005.03.001.
50. Bachler M, Schroeder R, Von Ahsen U. StreptoTag: a novel method for the isolation of RNA-binding proteins. RNA. 1999;5:1509–1516. doi:10.1017/S1355838299991574.
51. Nagy P, Vereb G, Damjanovich S, Mátyus L, Szöllősi J. Measuring FRET in flow cytometry and microscopy. Curr Protoc Cytom. 2006;38:12.8.1–12.8.13. doi:10.1002/0471142956.cy1208s38.